Kinematic Design and Analysis of a Morphing Wing

Matthew D. Stubbs

Thesis submitted to the Faculty of the
Virginia Polytechnic Institute and State University
in partial fulfillment of the requirements for the degree of

Master of Science
in
Mechanical Engineering

Charles F. Reinholtz, Chair
Harry H. Robertshaw
Daniel J. Inman

December 3, 2003
Blacksburg, Virginia

Keywords: Kinematics, Morphing Wing, Hyper-Elliptic, HECS, QBCLM,
Quaternary-Binary Cross Linked Mechanism, Smart Structures

Kinematic Design and Analysis of a Morphing Wing

Matthew D. Stubbs

(ABSTRACT)

In order to optimize the flight characteristics of aircraft, wings must be designed for the specific mission an aircraft will see. An airplane rarely has one specific mission, and therefore is usually designed as a compromise to meet many flight objectives with a single wing surface. Large-scale shape change of a wing would enable a wing design to be optimized for multiple missions.

Engineers at the National Aeronautics and Space Administration (NASA) Langley Research Center are investigating a new Hyper-Elliptic Cambered Span (HECS) wing configuration that may lead to increased stability and control, and to improved aerodynamic efficiency, during flight. However, during take-off and landing, a conventional wing design (not curved down) may be preferred. Thus a need has been developed for a wing whose contour can be changed during flight. The so-called "morphing" that is required has been limited by a lack of feasible design solutions.

One design concept is to use an adaptive structure, with an airfoil skin applied, as the shape-changing driver. Most designs of this kind require multiple actuators to control the changing shape. This thesis introduces a novel design for a morphing wing mechanism using a single degree-of-freedom kinematic chain. In this work, the concept is introduced with sufficient background to aid in understanding. The design tools developed include a synthesis procedure and a sensitivity analysis to determine the effects of manufacturing errors.

This work was funded by NASA grant number NCC-1-03017, administered through NASA Langley Research Center by Dr. Garnett Horner and Dr. Lucas Horta.

Acknowledgments

Much of this work was a collaboration, and the credit, therefore, deserves to go to many people besides myself. My fellow graduate students Will Whittier, and Leonard Wiggins, have helped develop many ideas presented here, and their help and amiability was an asset to the project.

However, it is our professors that are the ones deserving the most credit. Appreciation must be expressed to Dr. Charles F. Reinholtz – committee chairman, Dr. Harry H. Robertshaw, and Dr. Daniel J. Inman, of the Mechanical Engineering Department of Virginia Polytechnic Institute and State University. Their willingness to let me be involved in this project is greatly appreciated. Dr. Reinholtz, in particular, gave up much time of his own "vacation", opened his home as a workshop, and provided support and technical insight as was necessary.

Dr. Martin Day, of the Mathematics Department at Virginia Polytechnic Institute and State University helped me communicate the ideas expressed in Appendix A, and his help was tremendous for my own desire to understand the problem better.

The grant administered through NASA Langley Research Center by Dr. Garnett Horner and Dr. Lucas Horta (grant number NCC-1-03017) is also appreciated.

Finally, the best part of all – thanks to my bride, without whom I would not be complete. I appreciate all your encouragement and love. The great food at the presentation might be the reason I graduated!

Soli Deo Gloria.

Contents

List of Figures

List of Tables

Chapter 1

Morphing Wing Aircraft

1.1 The Hyper-Elliptic Cambered Span Wing

Engineers at NASA Langley Research Center recently developed hyper-elliptic aircraft wing configurations. These biologically inspired configurations, known as the HECS (Hyper-elliptic cambered span) wing, were developed as part of the Morphing Project in the Aerospace Vehicle Systems Technology Program. The two configurations of the wing shape, (Figure 1.1) consist of both a planar, and an anhedral, non-planar, configuration. All further discussion of these positions will denoted by the terms, "initial", and "morphed", respectively. In the initial position, the wing resembles a normal fixed wing, extending straight out from the aircraft. In the morphed position, however, the wing takes on a hyper-elliptic, curved down shape. Both of the configurations discussed, have a hyper-elliptic, swept back, leading and trailing edge.

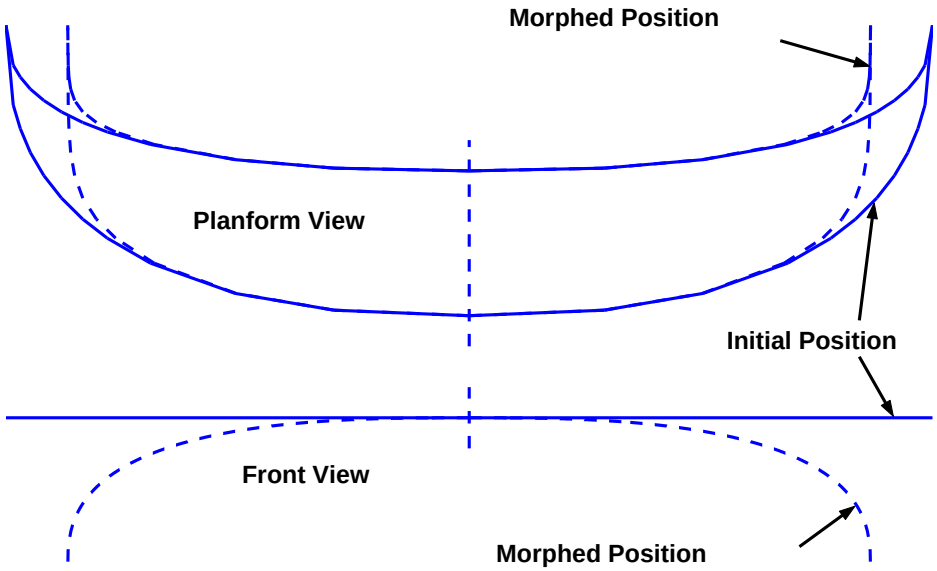

Figure 1.1: Layout of the HECS configuration

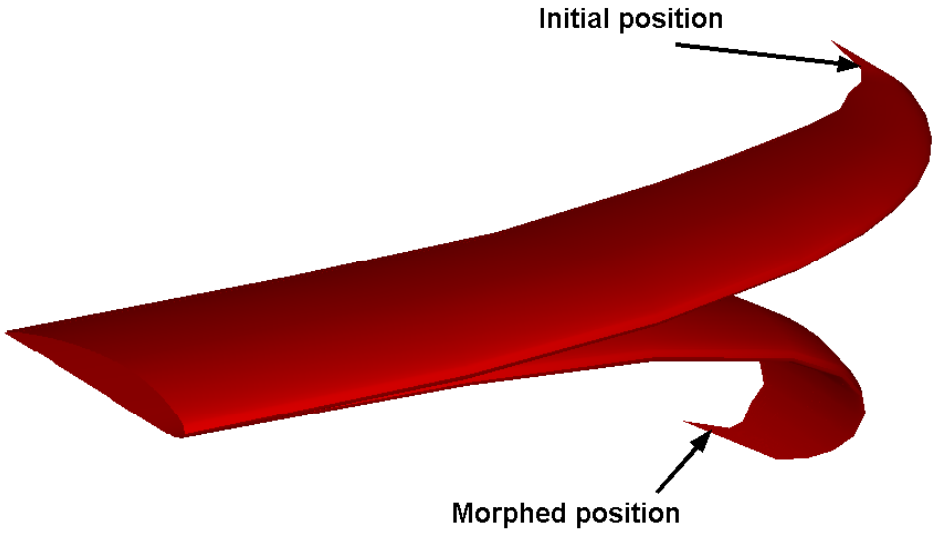

Figure 1.2: Initial and morphed positions for a single spar of the HECS wing

1.2 Motivation for Morphing

The ability to change the shape of a wing while an aircraft is in flight is desired for a number of reasons. Although there are other advantages from morphing wing technology,[1] the aerodynamic benefits of morphing can be considerable.

1.2.1 Wing Shape

When designing aircraft according to aerodynamics, shape is the most important characteristic. When a specific type of flight or mission is required, there is usually an ideal configuration of the aircraft to accomplish the mission [1]. For example, a certain wing shape might be ideal for the most fuel-efficient cruising, whereas a different wing shape would be ideal for high speed maneuvering. Another example is the use of flaps (that are deployed during takeoff and landing) to change the shape of a wing. Since the mission of an aircraft varies in flight, the wing chosen (for normal fixed wing aircraft) must be a compromise, giving reasonable performance for all possible missions. Although a change of the shape of a rigid wing is possible (using surfaces such as wing flaps, spoilers, ailerons, etc), these surfaces cannot produce the large-scale shape change that is needed to optimize flight characteristics in all missions.

1.2.2 Eliminating the Compromise

To eliminate the need to compromise wing shape design, recent research has focused on developing an aircraft wing that can morph, or change shape, during flight. Morphing implies a continuous variation in shape along the full span or chord of the wing. Common articulated flight control surfaces are excluded from this definition. In the future, it may be possible for a morphing wing to take on complex combinations of shape and size during a flight.

[1] Obstacle avoidance for un-manned air vehicles may be an application of morphing technology, for example

1.2.3 Flight Control and Mission Control

Two popular categories of current morphing research are flight control and mission control. Flight control morphing involves making relatively small adjustments in the shape of the wing to control the aircraft during flight. Mission morphing involves making major shape changes in order to optimize wing shape for a specific phase of flight. Although similar morphing technology may be useful for flight control in the future, this research focused on the mission morphing specified by NASA Langley. Hence, it assumed that conventional flight control methods (flaps, etc.) would be employed.

Some specific benefits associated with mission morphing of the HECS configurations have been previously shown. In work by Davidson, et al. [3], a wind tunnel test showed an increase in lift-to-drag, of as much as 15 percent for the HECS wing compared to a planar elliptic wing of the same aspect ratio[2] and wingspan. Although it is beyond the scope of this work to consider such benefits further, it is understood that morphing is required between the two configurations while the vehicle is in flight. The method of morphing the wing between the initial and morphed positions (in a predictable manner) is the subject of this work.

1.3 Past Research for Morphing Techniques

Various wing shapes have been developed and studied for possible morphed wing configurations. This research has focused on two distinct methods for wing morphing, namely, shape change of discrete chord sections and morphing the full spar of the wing in a more general manner. These two methods are discussed in more detail in the subsequent sections.

[2]The aspect ratio is the square of the wingspan divided by the planform area of the wing

1.3.1 Morphing of Chord Sections

One method of morphing is to change the shape of chord sections of the wing. If multiple chords sections are morphed in a specified manner, the shape of the wing, and therefore the aerodynamic characteristics of the wing, will change. Many ideas, including some kinematic concepts, have been proposed in the literature for this type of morphing. Both rigid link, and compliant mechanisms have been considered.

The Mission Adaptive Wing [17], developed on an F-111 test bed, is one concept that included rigid link mechanisms in the morphing of chord sections. This concept was developed under the Advanced Fighter Technology Integration program of the Air Force, to optimize flight characteristics at multiple aircraft speeds. It is shown in the above-referenced article how cambered configurations of aerodynamic lifting surfaces can cause parts of the air stream to reach the sonic range, even when the aircraft is flying at speeds as low as Mach 0.65. These high speed portions of the airstream cause airflow separation, and thus, an increase in drag can occur. To counter these adverse effects, an advanced airfoil (the so-called supercritical wing) design was developed. The results were reduced drag and a wing that can be designed for multiple speeds by changing the shape of the airfoil.

Similar research by Monner [8] showed how variable camber at the trailing edge can be realized. This interesting design employs both prismatic and revolute joints to change the shape of the chord section, which can be varied, differentially, along the spar. In the example given, Fowler flaps and ailerons are replaced with a smooth contour flap that yields many aerodynamic benefits.

"Compliant", simply means that a mechanism obtains mobility through flexure (at least partly), instead of through conventional joints. Of morphing concepts employing compliant mechanisms, Saggere's work [12] is an excellent example of shape control for chord sections. Two actuators (per section) are employed for shape control of both leading and trailing edges. Further advancement in the design of compliant morphing is expected as knowledge about topology optimization increases (see [2] or [13] for example).

These chord-wise morphing methods work well for specific problems, but it can be shown

that further shape change (including the shape change necessary for the HECS problem) will require different morphing methods.

1.3.2 Morphing Along the Entire Spar

To further generalize the possibilities of shape change, research also began to employ methods that actuate a greater extent of the wing. Twist control along the length of spar using Shape Memory Alloy (SMA) torque tubes, for example, has been considered. Quackenbush, et al., [9] and Jardine [5] have built wing tunnel models using SMA actuation. The positions, or shapes possible for a morphing wing, however, could be expanded even further.

1.4 Possible Research for Morphing Techniques

Whittier [18] explored tensegrity structures (see Figure 1.3) from a kinematic point of view, partly with the hope of using these structures to generate extensive shape change. According to Whittier,

> tensegrity structures consist of isolated compression members (rigid bars) suspended by a continuous network of tension members (cables).

A key concept to understand about tensegrity structures is that they only exist in certain singular configurations, according to their specific geometries. Other configurations will cause the structure to collapse as it gains mobility. These feasible configurations are actually boundaries of non-assembly. The conclusion, due to these complexities, is that tensegrity structures are not a viable option for actuating a morphing wing. Variable geometry trusses, however, do not have the stability problems associated with tenesgrity structures.

Although the joints in a truss can be quite complex (to allow each member, at a joint, to rotate freely with respect to each other member) the members need only to resist forces along their respective axis. These characteristics tend to lead to a configuration that is both strong and light. Actuating any member (through a change in length) causes the structure

Figure 1.3: Example tensegrity structure [Whittier, 2002]

to move correspondingly. This relation between actuation of members, to shape change, forms the basis of application of VGTs to morphing wings.

Salerno [10, 11] developed methods for shape control of VGT manipulators using order reduction methods to reduce extra DOFs during control. The literature review provided in Salerno's thesis is extensive, beginning with Stewart's [14] parallel manipulator research in 1965. One interesting note that Salerno mentions is the difficulty of controlling these manipulators. The multiple degrees of freedom require massive iterative algorithms and sophisticated control schemes. The benefit, however, of Salerno's work is that one may choose how a shape is approximated. The long-reach VGT manipulators shown in Figure 1.4 are "shape solutions" based on a given goal configuration. It is apparent that solution (b) requires fewer degrees-of-freedom than the other two solutions. At least three "sections" of this solution could be static truss sections, and this choice was possibly a user input.

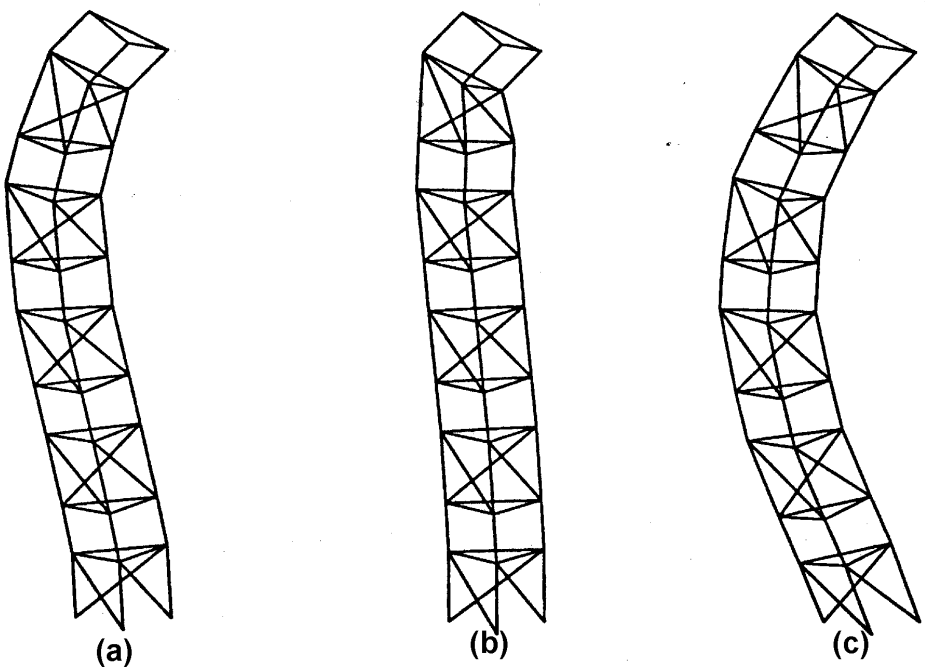

Figure 1.4: Three shape solutions for a given goal configuration [Salerno, 1993]

1.5 Single Degree-of-Freedom Concept

As can be readily seen, multiple degree-of-freedom (MDOF) mechanism concepts for morphing wings can be quite complex, heavy, and difficult to control. Instead of focusing on these MDOF concepts, this research focused on the design of a practical single degree-of-freedom (SDOF) morphing wing that can morph between two specific positions or shapes using a single actuator. The narrow focus of effort has lead to a design that is simple and easily controlled. Adaptability to retain some MDOF advantages, however, still remains, in that a more complex shape control can be realized through the actuation of any of the rigid members.

Chapter 2

Single Degree of Freedom Design

One morphing wing design concept is to use a multiple degree-of-freedom adaptive structure, with an airfoil skin applied, as the shape-changing driver. Most designs of this kind require multiple actuators, one to control each degree of freedom required. In this chapter, however, a novel design for a morphing wing mechanism, using a single degree-of-freedom kinematic chain is proposed.

2.1 SDOF Shape and Curve Approximation

Although many ideas have been presented for shape, or curve approximation using MDOF systems (see [11] for example), relatively few SDOF concepts exist that are capable of approximating a general shape, or curve. As mentioned in section 1.3.1, both conventional and compliant mechanisms have been used for active camber control (shape control) using a single degree of freedom on either the leading or trailing edge. In this case, the shape morphing was limited to a single airfoil section. In addition, Buhl's work on topology and shape optimization [2] shows that extremely intricate paths can be approximated using a single degree of freedom. However, neither of these concepts yield the form of morphing that is required for the current design.

In order to facilitate understanding of the adaptive structure developed, a review of some

basic kinematic chains is followed by an explanation of mechanisms that may be applicable to the type of morphing required in this case.

2.2 Parallel and Serial Chains

A parallel kinematic chain is formed when links are joined together in such a way, that there are multiple paths to ground from any link in the chain. An example of a parallel kinematic chain (shown in Figure 2.1 (a)) is a four-bar linkage. Every link in the system has two distinct paths to ground; these paths are expressed in Table 2.1.

Serial kinematic chains, common to robotics applications, are formed when rigid links are connected sequentially. In this case, from any link in the system, there is one distinct path to ground, and hence, one distinct path between links. An example of a serial chain is shown in Figure 2.1 (b).

A serial chain mechanism usually has many degrees of freedom, the number being defined by the number of links and the type of joints. In this case, actuation of some form (electric motor, hydraulic actuator, etc.) is usually required to be at a respective joint. In other words, $n-1$ actuators are needed to position n links.

In an effort to bring the actuation point back to ground, tendon-driven mechanisms were developed. Tendon-driven mechanisms remain MDOF mechanisms, but all actuation is brought to a single point, and can be attached to the grounded link. Tsai's work on tendon-

Table 2.1: Paths to Ground of a Four-Bar Parallel Mechanism.

Link	Path 1	Path 2
1	ground	ground
2	$2 \rightarrow 1$	$2 \rightarrow 3 \rightarrow 4 \rightarrow 1$
3	$3 \rightarrow 2 \rightarrow 1$	$3 \rightarrow 4 \rightarrow 1$
4	$4 \rightarrow 1$	$4 \rightarrow 3 \rightarrow 2 \rightarrow 1$

driven manipulators [15] is a good example of how to synthesize this type of mechanism.

Whereas tendon-driven manipulators remain MDOF mechanisms, "single degree-of-freedom coupled serial chain" SDCSC Mechanisms [6] bring actuation to the ground link, and become SDOF mechanisms. The reduction to a SDOF device is usually accomplished by using some type of tendon or chain. These mechanisms, therefore, are similar to tendon-driven mechanisms. Although developed for path following, and intended for assistive devices, these SDCSC mechanisms could be designed to generate specified shapes.

2.3 Serial Chains of Parallel Mechanisms

It is well known that SDOF kinematic chains can be formed from a serial chain of parallel mechanisms. In this section, serial chains of parallel mechanisms are introduced and discussed. Ultimately, the design proposed for the morphing wing application, the Quaternary-Binary Cross Linked Mechanism, is discussed.

2.3.1 Ternary-Ternary Mechanism

A common example of a serial-parallel chain with a single DOF is the scissor linkage used in man-lifts and extensional gates. A diagram of this linkage is shown in Figure 2.2. This mechanism has a slider-crank input and a series of crossed ternary[1] links. As can be seen from its topology, the mechanism consists of a serial chain of four-bar linkages, and each four-bar in the chain shares two links with the previous four-bar in the chain. For example, links 3, 4, 5, and 6 form one four-bar mechanism and links 5, 6, 7, and 8 form the next four-bar in the chain. From now on, each four-bar mechanism (although sharing links with other four-bar mechanisms) will be denoted as a "section" of a mechanism. A general form of the same topology is shown in Figure 2.3. The sliding motion of the prismatic actuator has been replaced with the rotating actuation of a binary link.

The relationship between sections (the need for one section to share links with the previ-

[1]Ternary implies three joints, or connections, to other links

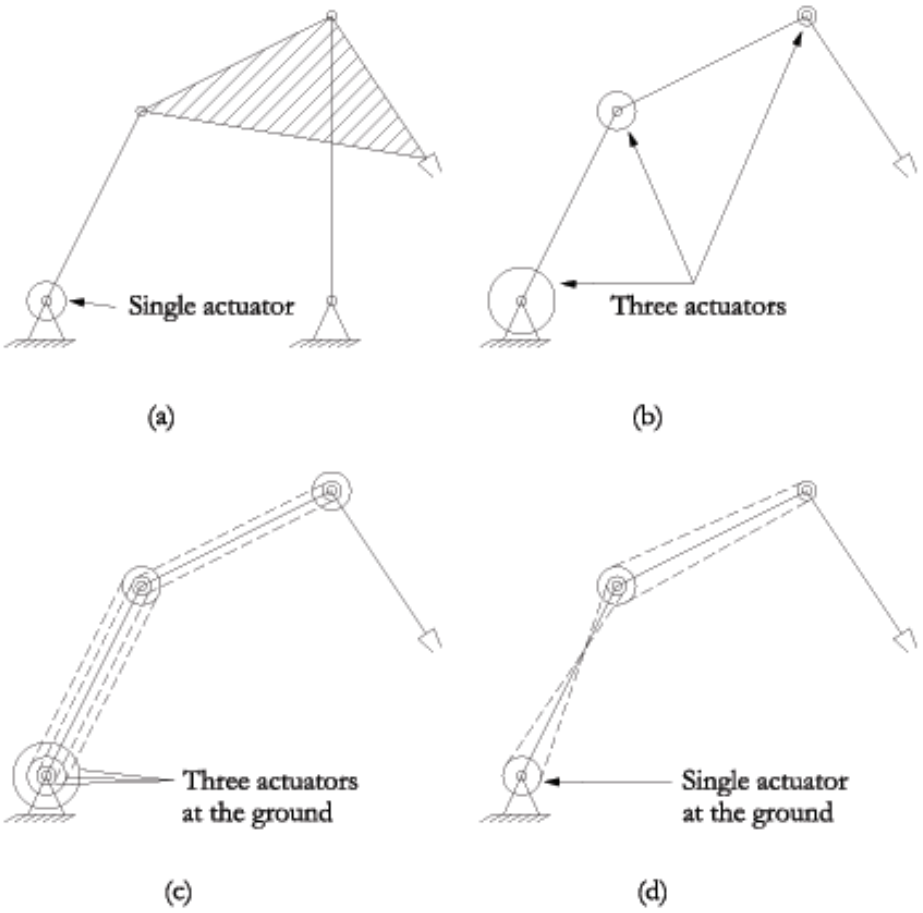

Figure 2.1: Relationship between some serial and parallel chains; (a) Four link parallel mechanism; (b) Three link serial mechanism; (c) Three link tendon-driven mechanism; (d) Three link "single degree-of-freedom coupled serial chain" mechanism [Krovi, et al.]

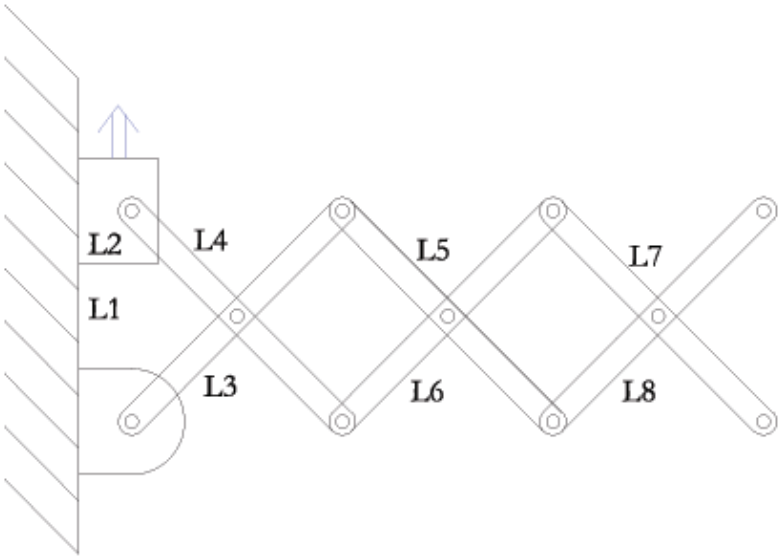

Figure 2.2: Ternary-Ternary Linkage (Scissor Mechanism)

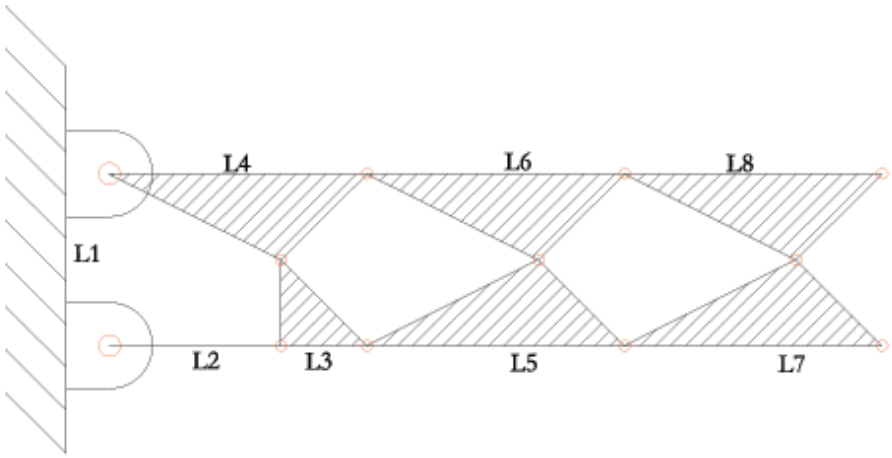

Figure 2.3: General Ternary-Ternary Linkage

ous section) can also be seen by considering the mobility of a planar mechanism. Grubler's mobility equation for lower pair mechanisms (from Erdman and Sandor [4] for example) requires that

$$M = 3(n-1) - 2f_1 \tag{2.1}$$

where the mobility, M, is found from both the number of rigid links, n, and the number of lower pair (revolute) joints, f_1. This implies that successively connected four-bar mechanisms, forming an articulating, expanding chain, must share rigid members to remain a SDOF device.

In a typical man-lift or extensional gate, the links of the scissor linkage have the same length. This produces the simple extension and retraction that is desired. However, if non-equal link lengths are specified, more complex motions or paths can be generated. Research on path optimization of mechanisms, including the scissor mechanism, may be useful for a morphing wing or for deployable structures [2].

2.3.2 Quaternary-Binary Mechanism

A second possible topology for a SDOF serial-parallel chain can be formed from a quaternary-binary link combination. The general form of this mechanism is shown in Figure 2.4. This mechanism is formed from a series of quaternary[2] links joined together with every other quaternary link connected through a binary[3] link. The mechanism does contain one ternary link, Link 2.

A kinematically equivalent quaternary-binary link mechanism is shown in Figure 2.5. In this mechanism the binary links cross the quaternary links in the same direction. The crossed link configuration forces all links to rotate in the same direction upon actuation. This mechanism will be hereafter referred to as the Quaternary-Binary Cross Linked Mechanism (QBCLM). An advantage of this kinematic topology is that the quaternary links can form a main articulating wing structure (similar to a manipulator), while the binary links are used

[2]Quaternary implies four joints, or connections, to other links.

[3]Binary implies two joints, or connections, to other links.

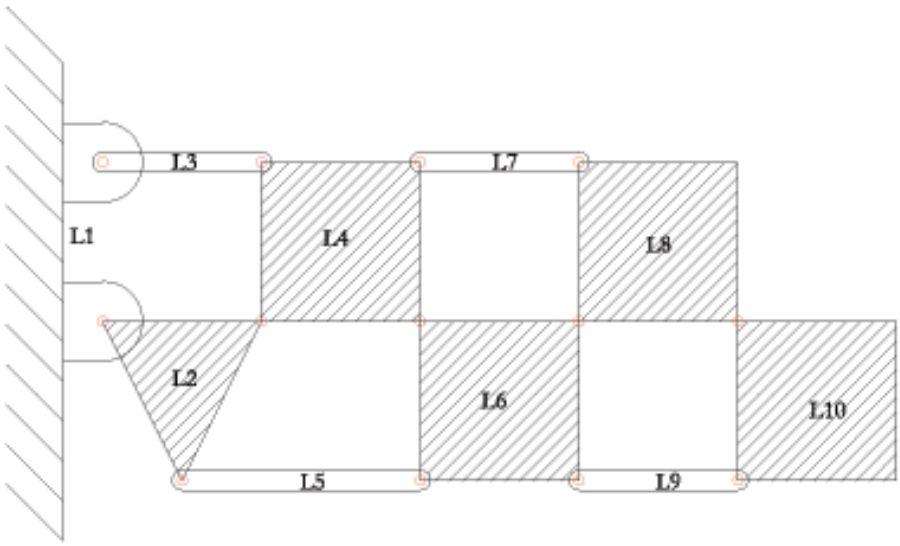

Figure 2.4: General topology of a quaternary-binary mechanism

to actuate the quaternary links. This arrangement allows the actuating binary links to be pure tension or compression members. Furthermore, the linkage can be designed such that the flight loads are borne by these members in tension only. These features will allow the mechanism to be both strong and light.

Examples of parallel, serial, tendon-driven, SDCSC, and QBCL mechanisms are shown in Figure 2.6 for comparison.

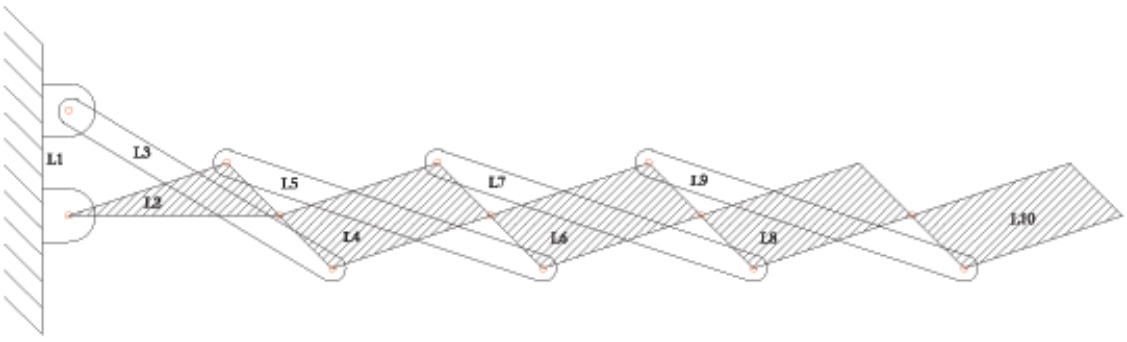

Figure 2.5: General topology of a quaternary-binary cross linked mechanism

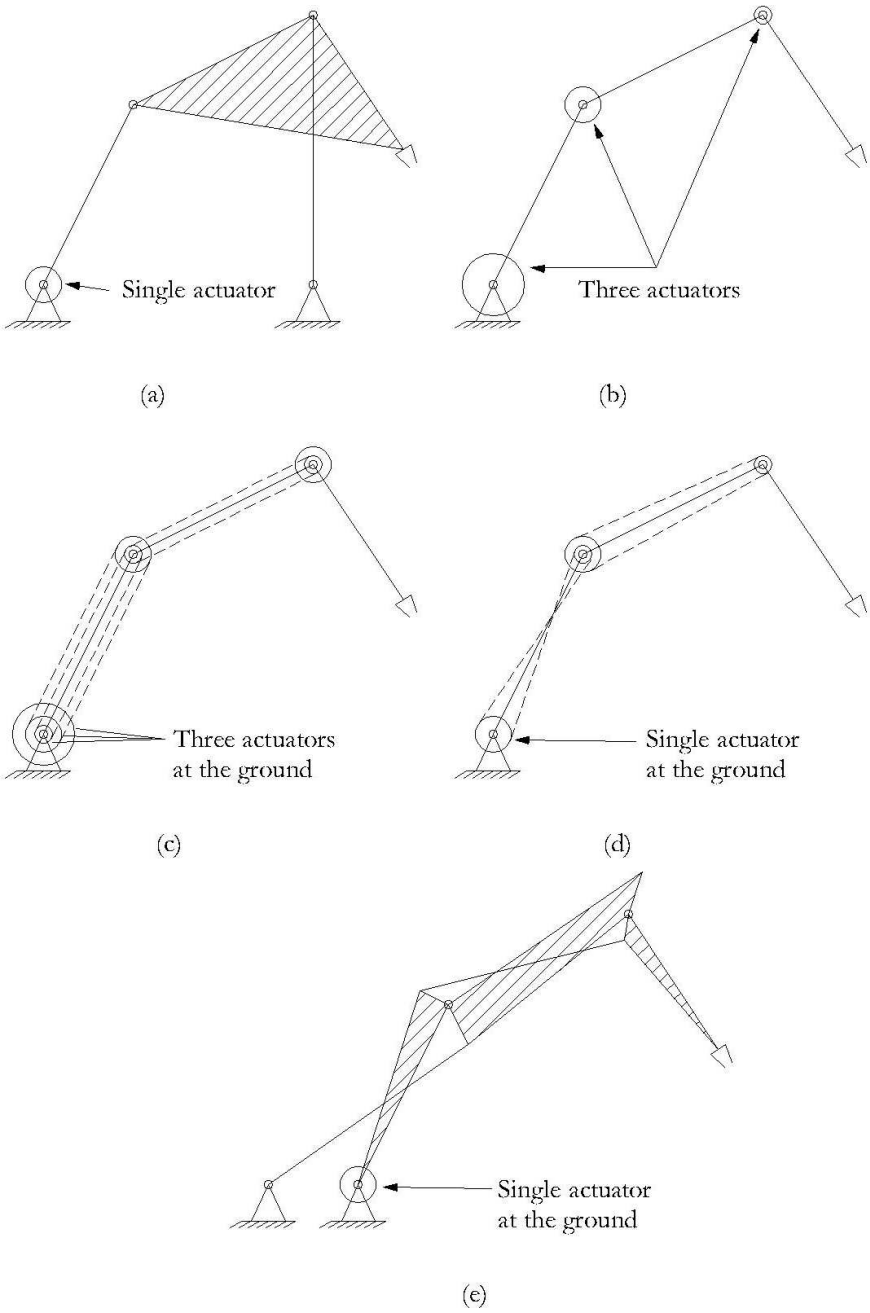

Figure 2.6: Comparison of both single, and multiple, degree-of-freedom mechanisms; (a) Four link parallel mechanism; (b) Three link serial mechanism; (c) Three link tendon-driven mechanism; (d) Three link "single degree-of-freedom coupled serial chain" mechanism; (e) Quaternary-binary crossed link mechanism

2.4 Synthesis

In this section, it is shown that it is possible to synthesize the QBCL mechanism to match the initial and morphed positions of the HECS wing configuration. In order to generate the required shape, the HECS curve is divided into sections, and the mechanism is then synthesized to match the required shape one section at a time.

2.4.1 General Curve Approximation

Any curve can be approximated using a series of discrete linear segments. The quality of the approximation will depend upon the type of curve to be approximated (linearity, order of non-linearity, etc), and the length and number of discrete linear segments used in the approximation. In the case of a linear curve the approximation may be exact, or include error. However, a finite series of continuous, linear segments, can only match a nonlinear curve at discrete locations. In the case of a non-linear curve defined as a hyper-ellipse, a continuous series of discrete linear segments are able to match the curve in at most, two places along the segment length.

2.4.2 HECS Curve Approximation

The approximation of the HECS configurations shown in Figure 2.7, was accomplished using the techniques discussed in section 2.4.1. Nodes, where the curve would be matched exactly (Figure 2.8) were chosen; these nodes became the endpoints of the series of discrete linear segments approximating the curve. This series of linear segments, and the resulting approximation, is shown in Figure 2.9.

The quality of the approximation generated using this technique is determined by the number of nodes, and the placement of these nodes along the curve. For example, it seems reasonable that shorter segments would be used in places where local curvature is high. Also, longer segments would be used at nearly linear portions of a curve.

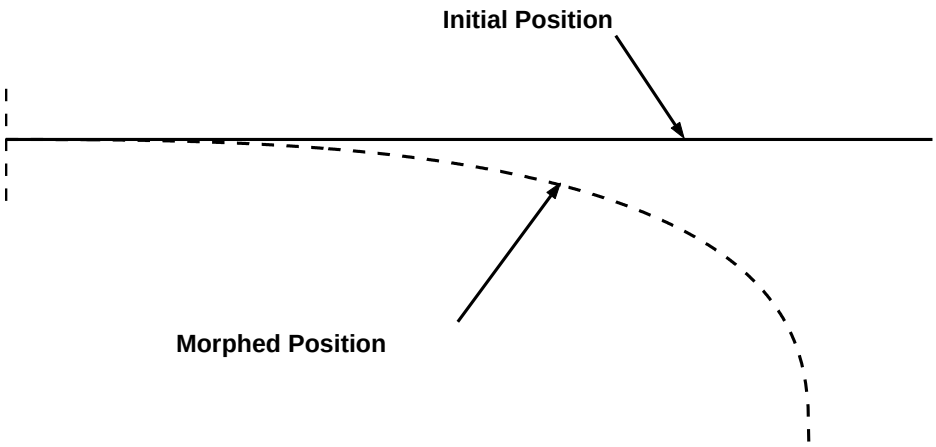

Figure 2.7: Front view of HECS wing configurations

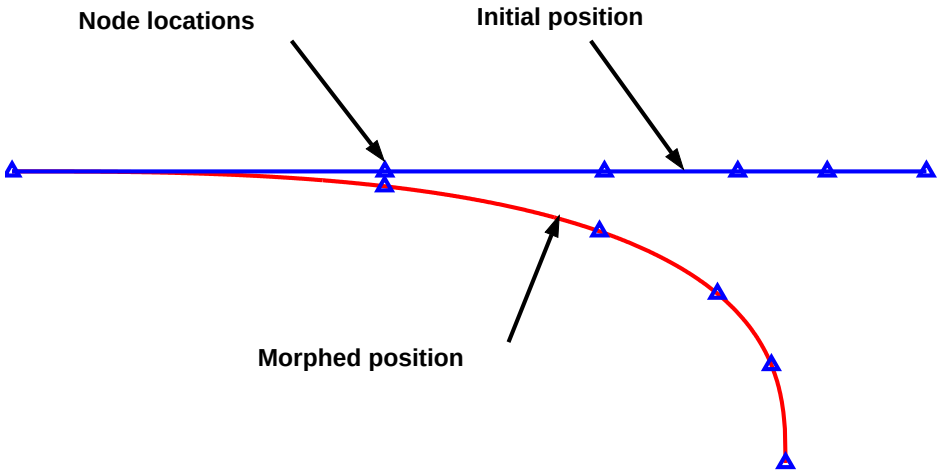

Figure 2.8: Nodes where curve is to be matched

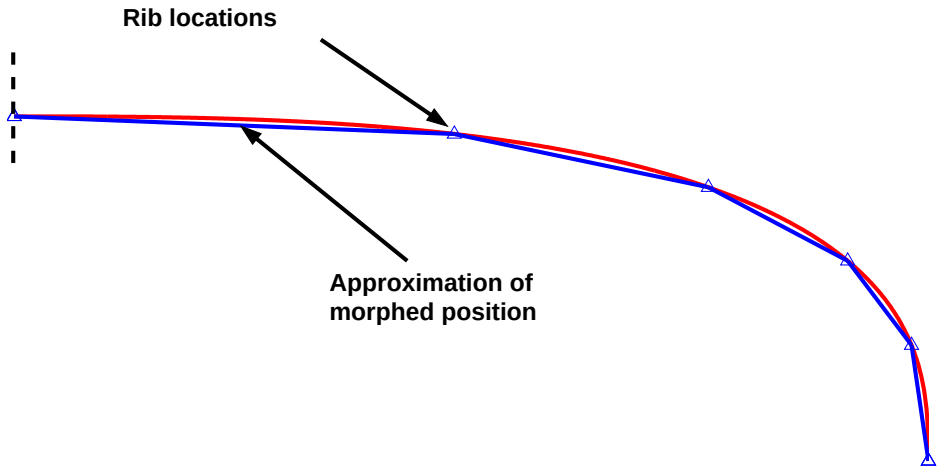

Figure 2.9: Approximation of wing shape based on number and placement of nodes

The goal in development of the QBCLM was to approximate the "shapes" or curves defining the initial and morphed positions of the HECS wing configuration shown in Figure 2.7. In this case, it is not imperative that the endpoints of the continuous linear segments be chosen for node locations. However, choosing the nodes to be at the segment endpoints proved to be an efficient manner of curve approximation. The nodes were chosen to represent two of the four joint locations on each quaternary link of the QBCLM. The linear segments then, represent the distance between these two joint locations. Therefore, the choice of the position and number of nodes, determines one part of the mechanism synthesis required for HECS approximation (see Figure 2.10).

It is interesting to note that both the value of n, and the choice of where the n segments match the curve, determine the maximum number of discrete places where the required shape is met exactly. For the choice of segments that have endpoints defined to be on the curve, the number of discrete locations, L, where the curve is matched is given by

$$L = n + 1 \tag{2.2}$$

Curve approximation for various of n is shown in Figure 2.11, where n is the number of segments chosen for curve approximation.

The nodes where discrete segments matched the curve were denoted as the "rib loca-

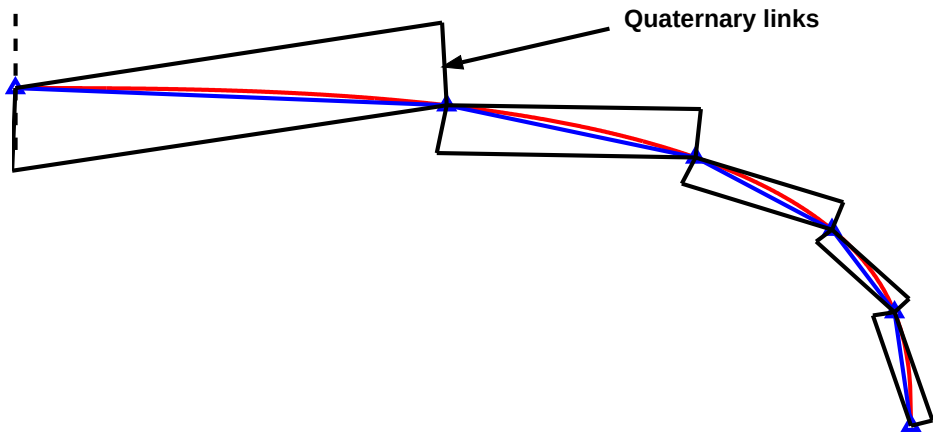

Figure 2.10: Node locations determine one dimension of each quaternary link

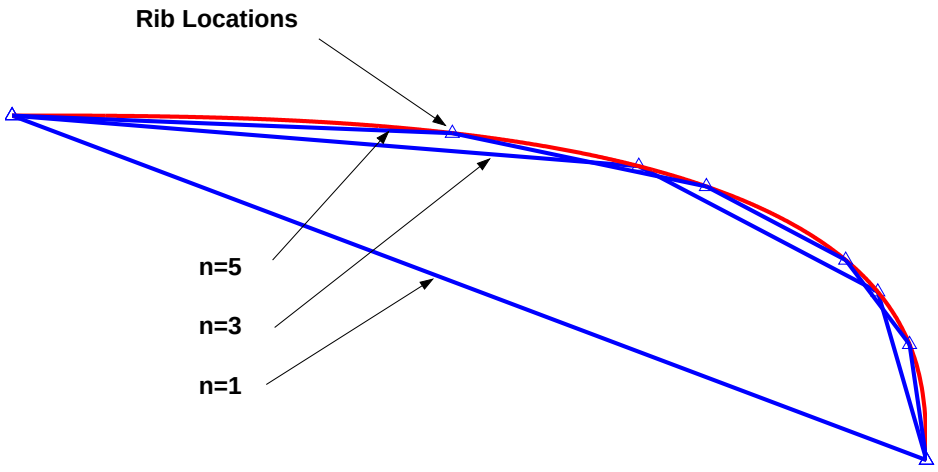

Figure 2.11: Approximations of HECS configuration for various n

tions." The rib locations were places where a rib, or airfoil section, is to be placed. Therefore, each airfoil section was placed exactly on the HECS curve, and any position along the spar that was not a rib location, had some error due to discretization. Thus, the discretization error is reduced as the number of sections (n) is increased.

The placement along the HECS curve, of the endpoints of these discrete segments is discussed in Appendix A. For the current design, engineers at NASA Langley specified eleven discrete segments, as shown in Figure 2.12. The specific segment lengths (and therefore rib locations) are considered proprietary information at the current time.

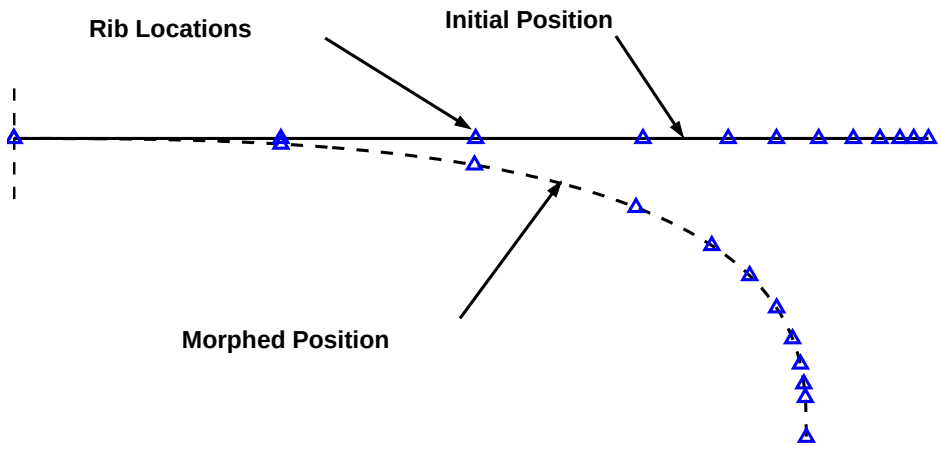

Figure 2.12: Rib locations chosen for synthesis

Given these eleven segment lengths, the goal was to synthesize a mechanism that matched the initial and morphed shapes. The initial case was trivial, as any arrangement of binary links can be made to force the quaternary links into a straight line (the initial position). The synthesis involved finding attachment point locations for the binary links that caused the motion to match the required end shape.

2.4.3 General Synthesis Approach

Synthesis of a mechanism involves proportioning the mechanism links to generate a required motion [7]. In this case, the required motion involves moving from an initial to a specified

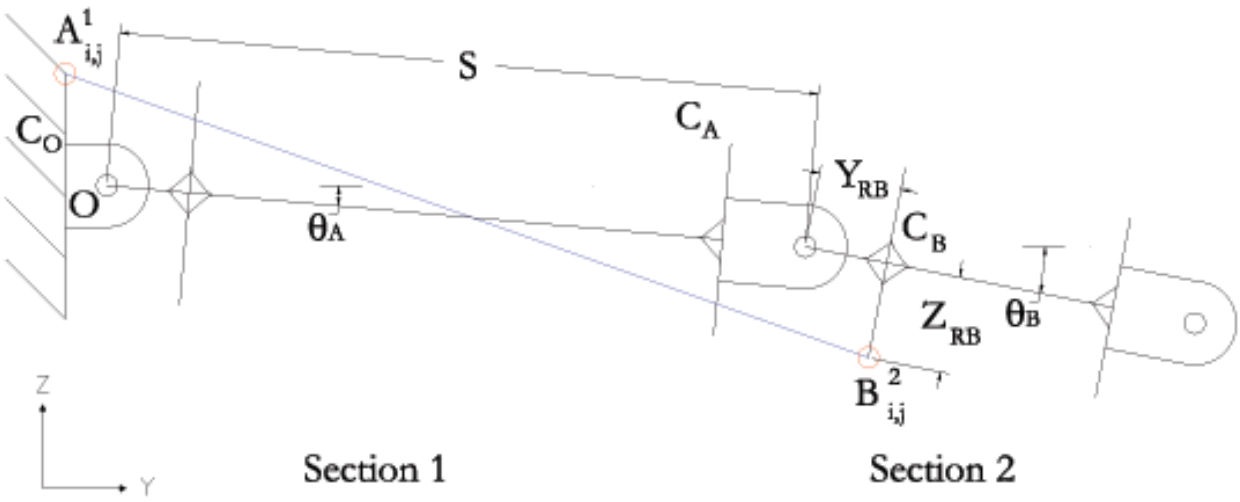

Figure 2.13: General synthesis notation

morphed shape. The goal then, was to develop a closed-form, or iterative method, of proportioning the QBCLM, that could be applied to the hyper-elliptic nature of the present required curve, as well as more general cases.

As mentioned in section 2.4.2, the segment length is important, but it is a free choice, and in this case, was specified by the sponsor. This segment length, for the case of synthesis was called the span, S, of a section. Each S was determined directly from Figure 2.12, while the other necessary proportions of the QBCLM were synthesized to meet the required morphed shape. These proportions were expressed as four design variables for each section, and consisted of the y and z locations of the binary link attachment points. Denoted as A, and B, respectively, these pivot locations are shown in Figure 2.13. Each four-bar section of the wing was synthesized separately, so the representation shown in Figure 2.13 is suitable for any two adjacent sections of the wing.

Near the ends of each segment of the QBCLM, a wing chord section could be attached. This chord section would be used to create the airfoil shape at a specific distance from the root of the wing. A skin could be applied between the chord sections. For synthesis it is required to know the vertical placement (the placement along the z-axis in the initial shape)

of pivot locations for the binary links. In the notation introduced in Figure 2.13, C_O, C_A, and C_B, represent the chord thickness at various locations along the span. C_0, represents the part of the segment that was assumed to be fixed to ground. In this case, C_0 represents the previous section in the chain for every section except the first. The C values comprised the largest thickness of a distinct chord section, and therefore the extrema of locations where pivot attachment points could be placed.

The cross-links for each section are defined from the location of the attachment points $A^k_{i,j}$, and $B^{k+1}_{i,j}$. In this notation, k denotes the section, and i and j specified if the wing was in the initial (i) or morphed (j) position. Y^k_{RB} defines the span distance between the section articulating point and the second attachment point B . Z^k_{RB} denotes the dihedral distance between the section articulating point and the second attachment point B.

Synthesis is performed by developing an expression for the location of the second cross-link attachment point, $B^{k+1}_{i,j}$. The distance between point 0, and B, is written in terms of its components:

$$\begin{aligned} y_{Bi} &= S + x_{RB} \\ z_{Bi} &= z_{RB} \end{aligned} \tag{2.3}$$

In the in the fully dihedral (j) position these become

$$\begin{aligned} y_{Bj} &= S\cos(\theta_A) + x_{RB}\cos(\theta_T) + y_{RB}\sin(\theta_T) \\ z_{Bj} &= S\sin(\theta_A) - x_{RB}\sin(\theta_T) + y_{RB}\cos(\theta_T) \end{aligned} \tag{2.4}$$

where $\theta_T = \theta_A + \theta_B$.

In order for the binary link to be considered rigid, its length in the initial and morphed positions, L_i and L_j, must be invariant. Expressions for these lengths are given in Equation 2.5:

$$\begin{aligned} L_i &= \sqrt{(y_{Bi} - y_A)^2 + (z_{Bi} - z_A)^2} \\ L_j &= \sqrt{(y_{Bj} - y_A)^2 + (z_{Bj} - z_A)^2} \end{aligned} \tag{2.5}$$

Constraining $L_i = L_j$ allows one to solve directly for points y and z for each section

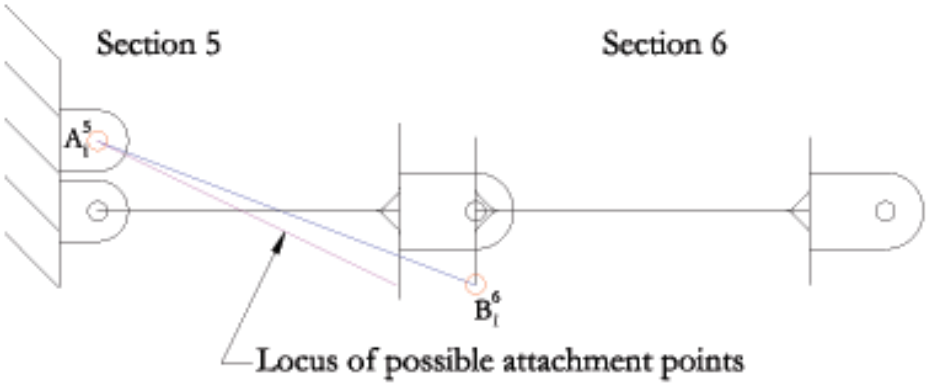

Figure 2.14: The locus of possible attachment points for A^5, given B^6 as shown

of the mechanism. This generation of y and z completes the basis for the synthesis. This technique was incorporated into a numerical code, which has been included as Appendix B.

At this point, constraining L_i and L_j to remain equal left three infinities of solution (one infinity being taken away from the original four infinities of y and z locations of both attachment points). There were, however, some constraints that limited the number of choices to one infinity of solution.

It was desired that the mechanism be contained within the airfoil volume. Therefore, constraints were placed on A and B, so that they lay within the area defined between the chord heights and the respective section span. Point B was chosen to lie at the extreme position $(S + Y_{RB}, -\frac{C_A}{2})$. Two infinities of solution were removed when this choice was made, but as a result, a mechanism with a maximum allowable section height was produced. Choosing the largest section height ensured that the mechanism had the largest cross-section to resist bending moment.

One infinity of solution still remains, and therefore a locus of possible pivot locations for A existed. As an example, for the fifth section in this mechanism, and for B fixed at $(S + Y_{RB}, -\frac{C_A}{2})$, the locus of possible attachment points (A) lies on the line shown in Figure 2.14.

For the final choice, point A was generally constrained to lie directly above 0. The

position of A along the x-axis was chosen for the same reasons that B was placed in its position, namely to produce the mechanism with the largest section height. A single solution for the location of point A along the y-axis was then found using a root finding technique. The remaining sections were synthesized in this manner and by sequencing through the sections to find all A_{ij}^k.

Sometimes A_x could not be chosen to lie directly above O. For example, occasionally this choice forced A_y to be greater than C_0, and, therefore, forced A out of the wing volume. In this case, A was chosen as the extreme point just inside the wing volume.

It was not assumed that all curves would require the same constraints of attachment points A and B. It may prove that other choices would generate a mechanism with the largest section height if the wing shape curve to be matched had points of inflection for instance. If the curve did have points of inflection, some sections of the mechanism would turn out to have binary links crossed over the quaternary links, and some would not. The benefit of this technique, however, is that each section is synthesized separately, and these "free choices" can be made differently for each section.

2.4.4 Alternate Body Guidance Approach

The unique manner in which the previously presented synthesis methods were developed is due to the physical constraints of the morphing wing mechanism. A similar approach to the synthesis can be developed by expressing the design parameters in terms of the link lengths shown in Figure 2.15. In this synthesis development, link 1 could be a grounded link, or a link that is shared with a previous section. For either case, the link can be designated as a grounded link, since the position of the previous section determines the position of the section being synthesized. In other words, if link 1 is not a grounded link, then its required motion is deduced from the kinematics of the previous section. Link 2 is the input link for this mechanism; it is actuated by the previous four-bar mechanism in the chain, or the main actuator if the section being synthesized is the first section of the mechanism. Rotating link 2 (of the first section) downward by a prescribed angle causes the entire mechanism to move.

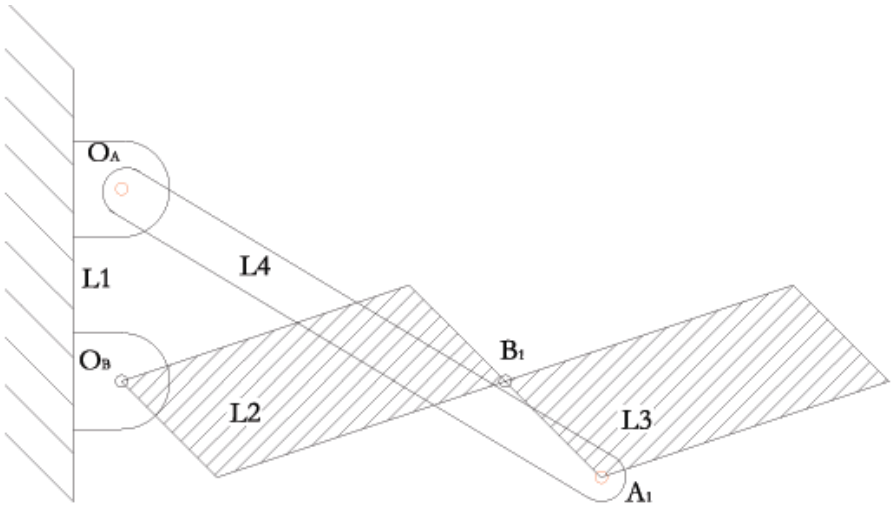

Figure 2.15: An example section extracted from the QBCLM

The output link (link 3), will also rotate downward to a specific angle determined by the geometry of the mechanism. Link 3 will serve as the actuation to the next section in the chain, and this process repeats.

This synthesis formulation results in the classic body guidance problem (clearly laid out by Mabie and Reinholtz [7] for example) in which the position and angle of each quaternary link is specified in two positions. Various techniques to solve the two-position body-guidance problem are well known in the literature. While this synthesis approach is more conventional than the one developed in section 2.4.3, it lacks a direct physical relationship to the parameters associated with the design of the morphing wing.

2.4.5 Synthesized Design

The synthesized morphing wing mechanism is comprised of the same eleven sections shown in Figure 2.12. When the eleven sections of the QBCLM are fully synthesized and used in the morphing wing, the wing structure becomes a parallel-serial, SDOF device. Link 1 of the first section is grounded to the fuselage, and actuation occurs by rotating link 2. The positions of links 1 and 2 specify where links 3 and 4 must lie. Links 3 and 4, then, are shared

with the next section, becoming links 1 and 2, respectively of section 2. In this way, each subsequent section has a defined position specified by the position of the previous section. Therefore, given the piecewise continuous curves defining the starting and morphed wing shapes, this synthesis technique can be used to produce a shape changing, or morphing, mechanism.

2.5 Conceptual Design

A simple skeleton model of the first four sections of the HECS morphing wing mechanism was built to validate the synthesis technique. Link 2 of section 1 was attached to a fixed rigid body (simulating the fuselage) by a revolute joint, and is then actuated by plate attached near the base joint. A picture of the model in an intermediate position is shown in Figure 2.16. The first section is shown clearly in Figure 2.17.

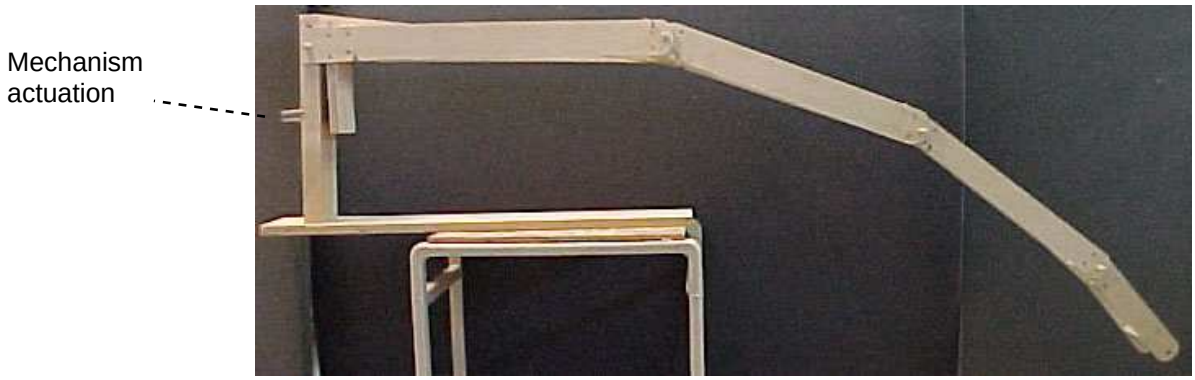

Figure 2.16: First four sections of conceptual model in an intermediate position

This model, and the design concept considered so far, approximates the required motion, but it will not fit inside the wing shape designated by NASA. The mechanism designed does not follow the sweep of the leading and trailing edges of the HECS configurations. The addition of sweep to the mechanism is introduced in section 2.6.

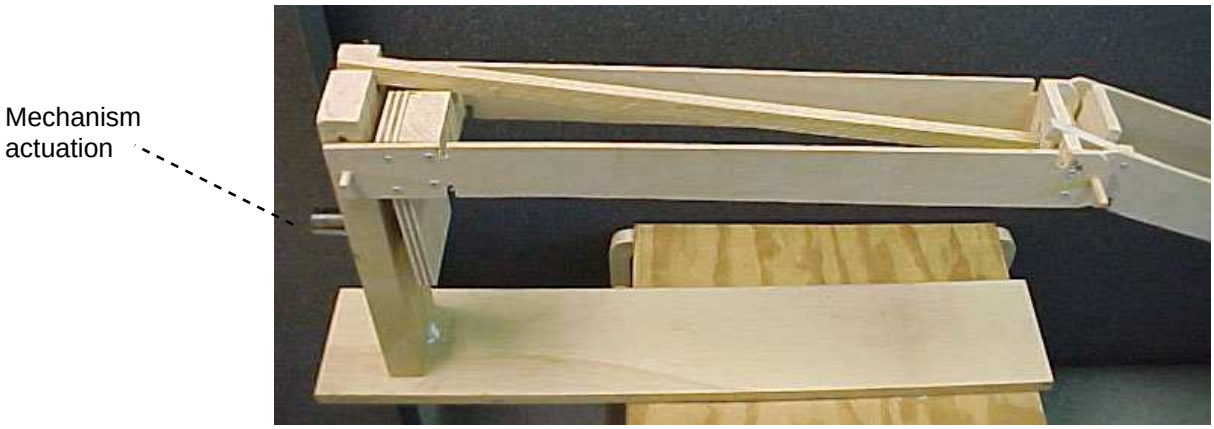

Figure 2.17: First section of conceptual model

2.6 Swept Design

As mentioned in section 2.5, a mechanism proposed for morphing of the HECS wing must take into account the hyper-elliptic nature of the sweep of the leading and trailing edge. The model shown in Figure 2.16 demonstrates the basic concept, but it has two flaws. It is a planar device, and it will protrude out of the volume of the spar. The next section introduces a model that includes the sweep of the HECS wing.

2.6.1 Sweep of the HECS Wing

The design of the HECS wing as proposed by NASA Langley, and shown in Figure 1.1, has a swept shape. From a planform view (as shown) this sweep does not change as the wing moves between the initial and morphed positions. Some change in mechanism design was necessary for the mechanism to remain inside the volume of the swept wing.

2.6.2 Constraining Mechanism Volume

In order to define the mechanism to fit inside the HECS wing, a constraining volume was generated for each section. Similar to the constraint on attachment points A and B in the

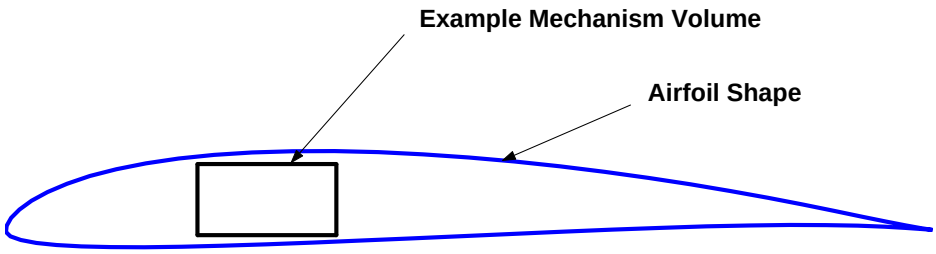

Figure 2.18: Example of constraining mechanism area in a chord section

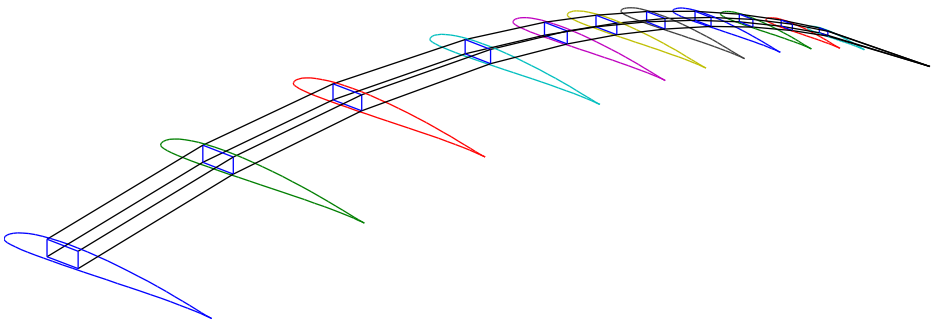

Figure 2.19: Constrained mechanism volume in initial position

conceptual design, constraints were placed on where the binary links were attached. This arbitrary volume consisting of the "usable area" of a chord section (shown in Figure 2.18), extended through all chord sections to create a volume (shown in Figures 2.19, and 2.20). Since the mechanism was defined to be, at all times, within these constraints, there was no protrusion of the mechanism into the air stream.

From Figures 2.19 and 2.20, it can be seen that the final mechanism design has similar motion to the conceptual design in the $y-z$ plane. This motion, however, is constrained to be in successively offset (yet remaining parallel) $y-z$ planes. This is explained further in section 2.6.3.

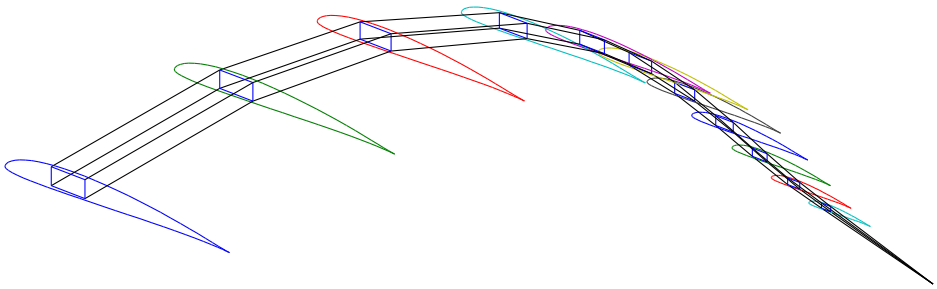

Figure 2.20: Arbitrary mechanism volume in morphed position

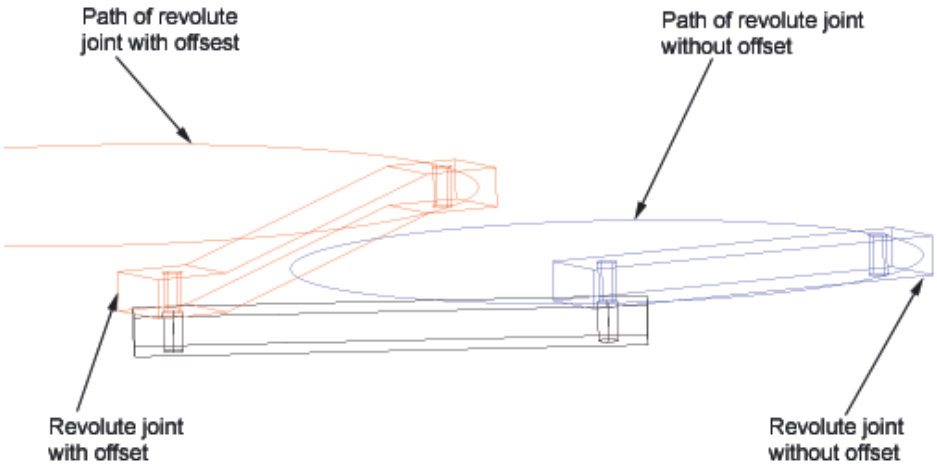

Figure 2.21: Comparison of motion of two revolutes

2.6.3 Mechanism Application

Planar by Section

Tsai [16] defines planar motion only to occur when the motion of all particles in the rigid body are constrained in parallel planes. This parallel motion is seen by comparing the motion of a pin joint in two-dimensional space, and a revolute joint with angular offset in three-dimensional space (see Figure 2.21). The planes of motion of the two links shown in Figure 2.21 are offset, but still remain parallel to each other. According to Tsai's definition then, the QBCLM will remain a planar mechanism, even when in a swept back configuration.

Synthesis

Since the mechanism remains planar, the synthesis method applied to each section remains the same. Therefore, the synthesis previously described (along with systematically changing planes of motion due to sweep) are valid in this case as well. The Cartesian position of the attachment points is given as

$$A^k_{ij_{Swept}}(x, y, z) = A^k_{ij_{UnSwept}}(y, z) + \sigma^k \tag{2.6}$$

where $A^k_{ij_{Swept}}$ (the attachment point location for the swept design) is a function of x, y, and z. It is obtained by adding the section offset, σ^k, changing the position of A only in the x direction. The change was similar for all eleven sections of the mechanism, as each section was sequentially swept back. In this case, σ^k was assumed to be the total offset from the initial section.

2.6.4 Synthesized Design

A fully swept linkage model similar to the conceptual design discussed in section 2.5 was constructed. The design details of this full-scale model are discussed in this section.

Quaternary Members

Wooden 1"x4" sections were employed as the main structural members. These quaternary members were attached serially using simple hinges, with the first section attached to a vertical member (using a simple hinge as a revolute joint), acting as the fuselage of the aircraft. Attaching rectangular sections together in a serial manner would have produced a similar mechanism to the one shown in section 2.5. Instead, to create the mechanism sweep, the sections were cut into parallelograms with the ϕ^k being the angle of sweep of section k. The shape of the wooden sections (see Figure 2.22), and placement of the hinges along the sections, forced all movement to be in parallel, yet successively swept back, planes.

In order to form these sections into the required quaternary links, binary link attachment points were secured to the sections at locations matching the synthesis results.

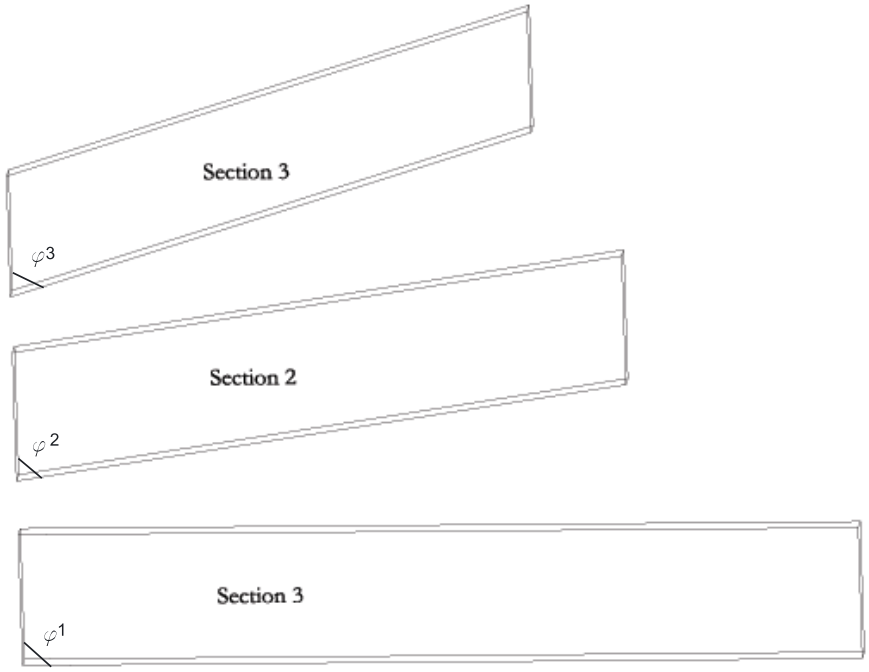

Figure 2.22: Size comparison of the first three sections of swept model

Finally, actuation was provided by a jack plate and bolt attached to the first section. The actuation point was simulated as being attached to the fuselage. A planform view of this model is shown in Figure 2.23.

Binary Members

In this model, (see Figure 2.24 for clarity) the binary links are two-force members. The binary members consist of tubing with spherical joints at each end. These joints allow no resistance to moments; therefore, they transfer no moments to the binary links. These constraints cause the members to carry axial loads only.

Binary Link Attachment Points

The attachment points A and B between the quaternary links and the binary link were made from brackets bent out of steel plate. Spherical joints were attached in between two

Figure 2.23: Planform view of model showing sweep of mechanism

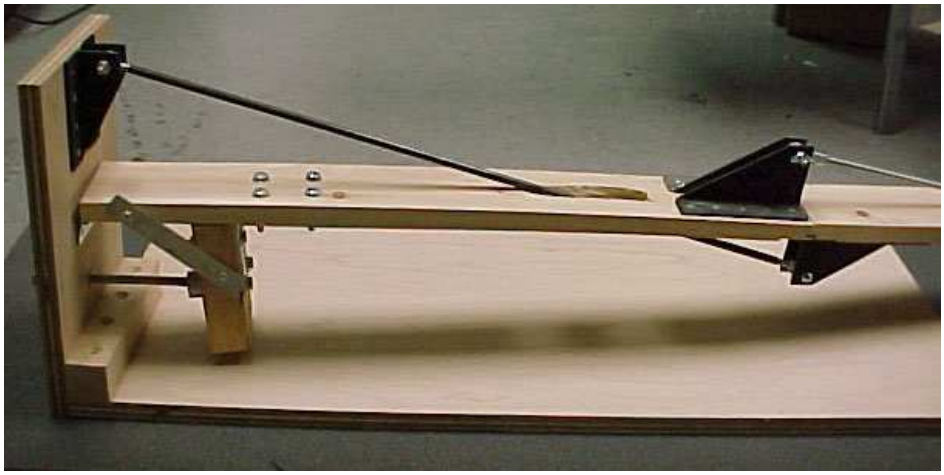

Figure 2.24: First section of swept model

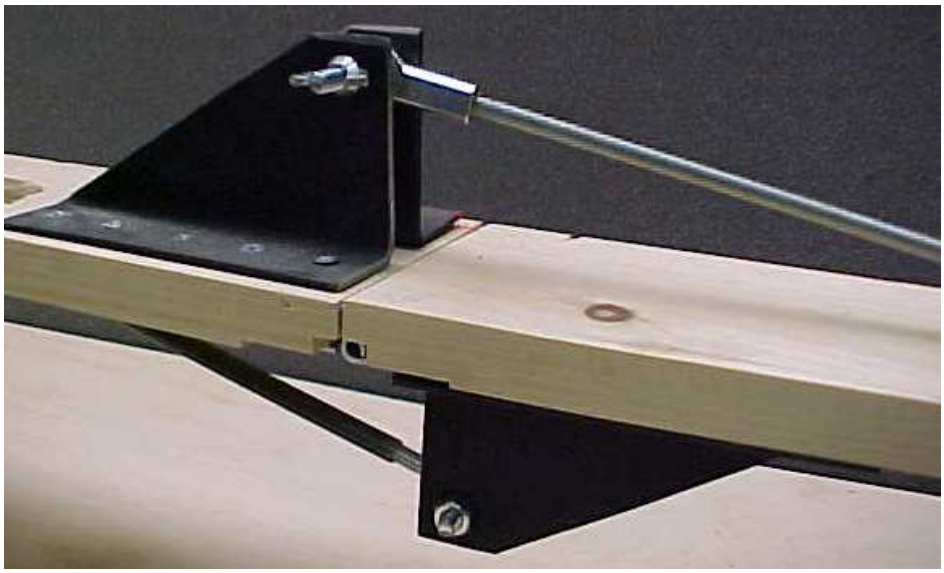

Figure 2.25: Example of original attachment point

mirror image brackets, and the binary link passed through a hole in the wood to another set of brackets on the opposite side of the next quaternary link. Although these brackets provide space for large rotations of the binary link about the bolted axis (see Figure 2.25), this initial bracket design did not allow for proper side-to-side motion of the binary link as the successive sweep required in each section.

Instead of placing the spherical joint between two upright brackets, a better design may be to place the spherical joint on an angled block. This concept was demonstrated using a combination of an angled wood block and a bent steel plate, which were both then bolted to the wooden section (see Figures 2.26 and 2.27).

2.7 Design Conclusions

The swept design went further than the conceptual design by generating the required shape in both the front and planform views. This was done using a SDOF mechanism that remains planar at each section, but obtains spatial characteristics through the section sweep, ϕ^k. It

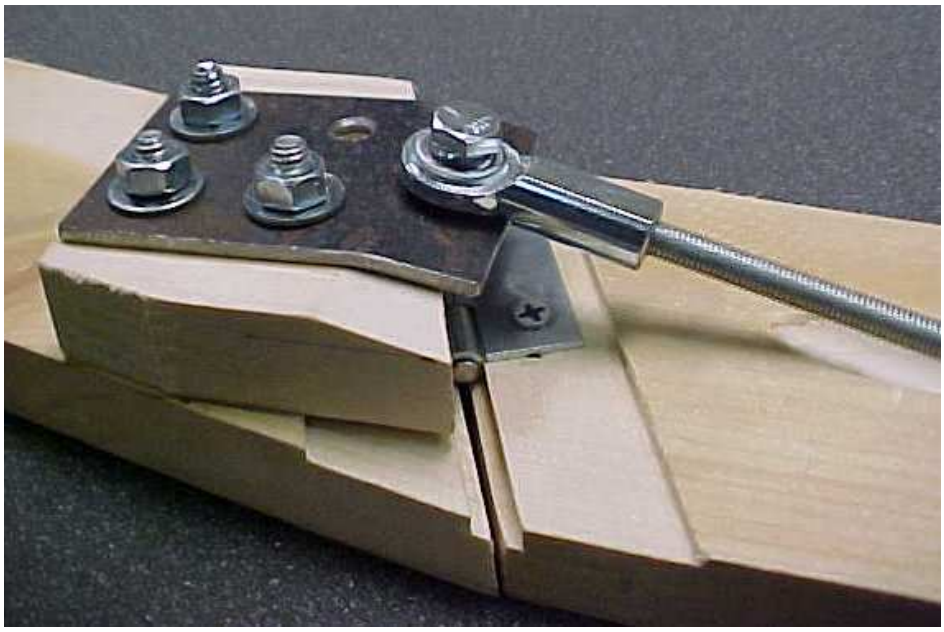

Figure 2.26: Example of proposed attachment point, as attached to underside of mechanism

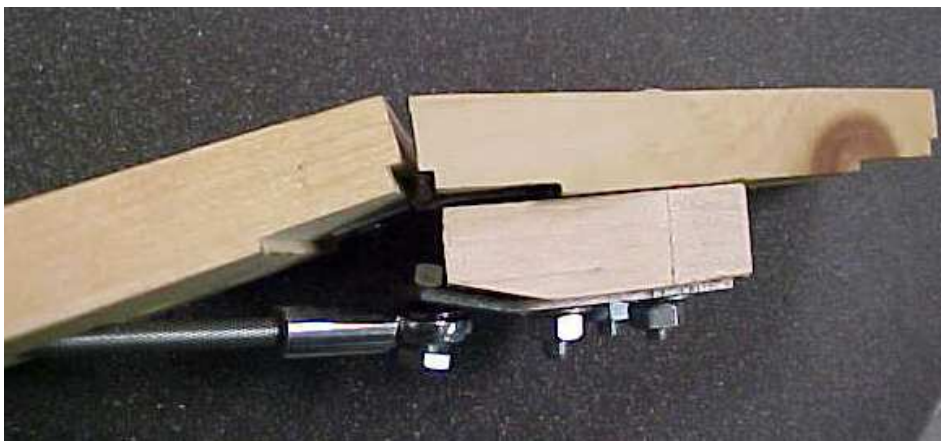

Figure 2.27: Second example of proposed attachment point

is proposed that wing sweep can be adjusted in flight, by adjusting the sweep angle ϕ^k of the wooden sections (see Figure 2.22, and Appendix C).

Chapter 3

Sensitivity Analysis

To morph the wing from an initial position to the fully morphed position, the input link of the mechanism (link 2) must be rotated less than 3 ° relative to the base. Because the motion in each section is relatively small, a concern was raised about the sensitivity of the design to manufacturing error and link compliance. In order to quantify the ability of the mechanism to match the given shape in the presence of error, a sensitivity analysis was performed.

It is assumed that a small amount of error can be expected from any manufacturing process. This manufacturing error can be categorized into two distinct types: "bias" and "random machining" error. Bias error, causing all links to be too long (or too short, respectively), is assumed to be controllable, and therefore, will not be considered. A random error due to inaccurate manufacturing has been considered. The effect of random error on the capability of the mechanism to generate the required morphed shape was determined using a Monte Carlo simulation. For this study, it was assumed that a machining practice capable of producing links of the Morphing Wing mechanism could hold tolerances of $\pm 0.005 in$ normally distributed about the mean. It is also assumed that this tolerance could be held within 3 standard deviations. Although analytic methods could be employed to generate the sensitivities of the mechanism response to the design variables, a computer generated Monte Carlo study was chosen.

3.1 Definition of Error

Error in the final wing assembly was defined using a combination of two physical measures (linear error, E_L, and angular error, E_A):

$$E_L \equiv \left\| P - P_{RE} \right\|_2 \tag{3.1}$$

$$E_A \equiv \theta_{2(11)} - \theta_{2(11)_{RE}} \tag{3.2}$$

These error measures were defined to be the difference in tip position and tip orientation between a flawless wing and a wing with random error, RE, included in the link lengths. E_A denotes the angular error of the last section of the wing, while E_L denotes the linear error of the most extreme point along the span of the wing. These errors are shown in Figures 3.1 and 3.2.

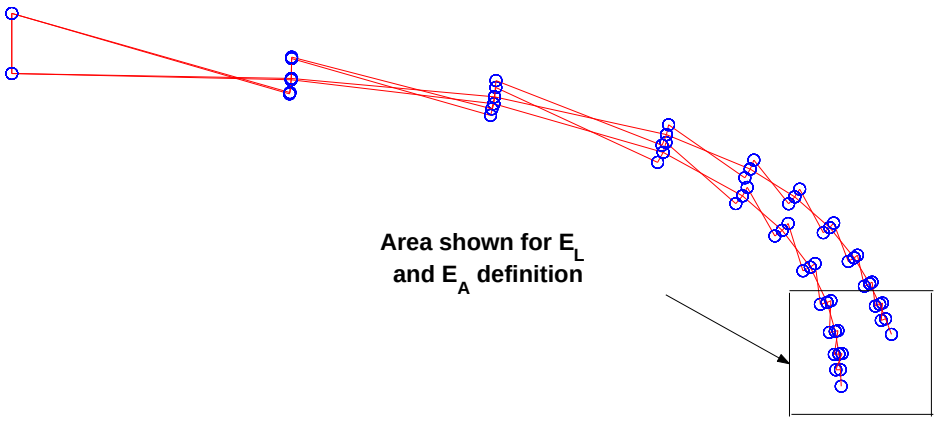

Figure 3.1: An example of mechanism error due to manufacturing

3.2 Method

Sensitivity code was developed for the analysis using Matlab. Normally distributed random error was applied to each of the 24 links, and the end errors, E_A, and E_L, were calculated according to Equation 3.1. To obtain the expected distribution of the end error for any

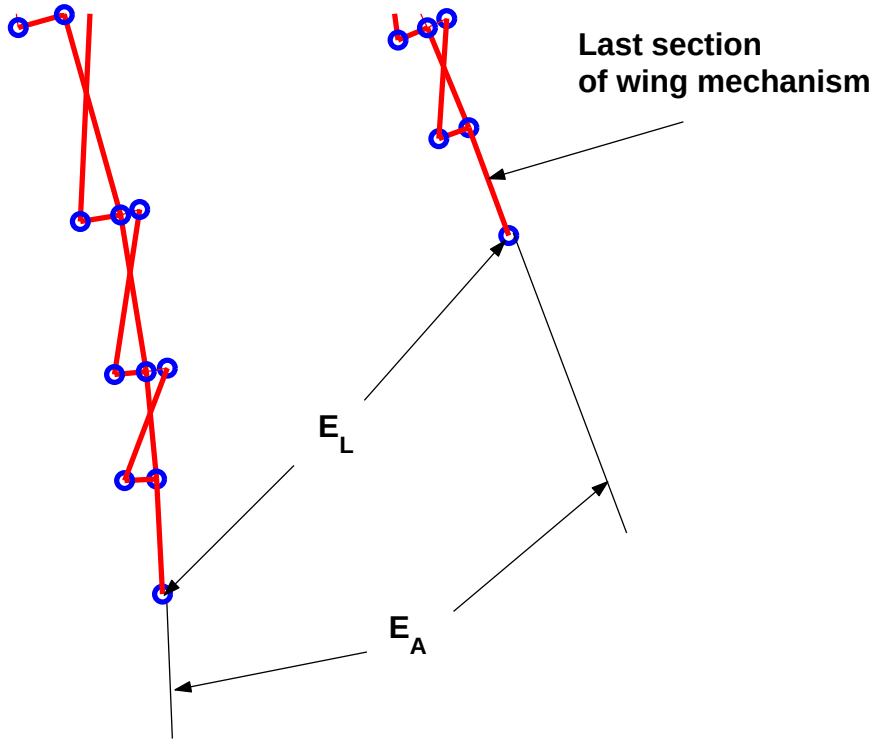

Figure 3.2: Definition of end error measures, E_A and E_L

mechanism after machining, random error was applied to the link lengths 100,000 times. An end error was calculated for each of the 100,000 simulations.

3.3 Results

The mechanism links were specified from the closed form kinematics, and the position errors were calculated for the 100,000 random error applications. Maximum positive and maximum negative errors are shown in Table 3.1 along with the standard deviation of the calculated error. Representations of these errors for both the initial and morphed positons are discussed in sections 3.3.1 and 3.3.2.

Table 3.1: Properties of Error Measures.

Error Measure	Mechanism Position	Maximum Negative Error (deg, in)	Maximum Positive Error (deg, in)	Error Standard Deviation (deg, in)
E_A	Initial	-11.2794	13.2719	2.9547
E_A	Morphed	-8.7785	9.5043	2.2106
E_L	Initial	-3.2371	3.3797	0.8517
E_L	Morphed	-2.4121	2.8052	0.6447

3.3.1 Angular End Error

The angular end error, E_A, was measured in degrees and was calculated for both the initial and morphed positions. For both positions, the maximum error, and error standard deviation are given in Table 3.1, while the characteristics of the error can be better seen in Figure 3.3.

Quantile-quantile (Q-Q) comparisons have also been included (see Figure 3.4, for example). A Q-Q plot is used to compare the distribution type of two data sets. In this case, the data sets compared are the input manufacturing error to the link lengths and the output position errors of the mechanism. Note that angular error in this position has the same distribution as the input data (as shown by the Q-Q plot in Figure 3.4 by the tight fit of data points along a straight line). Therefore, normally distributed random machining error is expected to yield normally distributed random error in the ability of the mechanism to approximate the wing shape.

For the morphed position, the results were similar, but they were found to have smaller standard deviations (see Table 3.1). The smaller value of standard deviation implies that the mechanism error in the morphed position has a tighter distribution about the mean error. This tighter spread, and overall smaller magnitude of error, can be seen in the histogram of Figure 3.5.

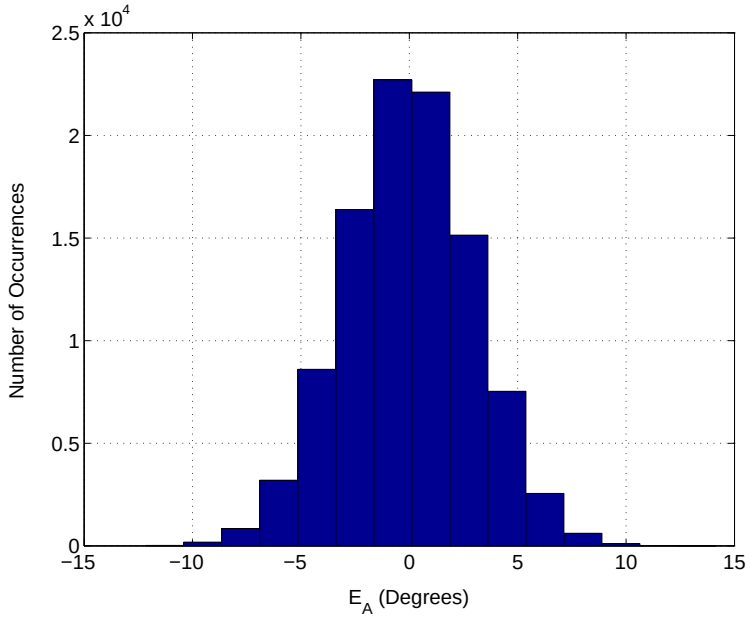

Figure 3.3: Histogram showing E_A for the wing in initial position

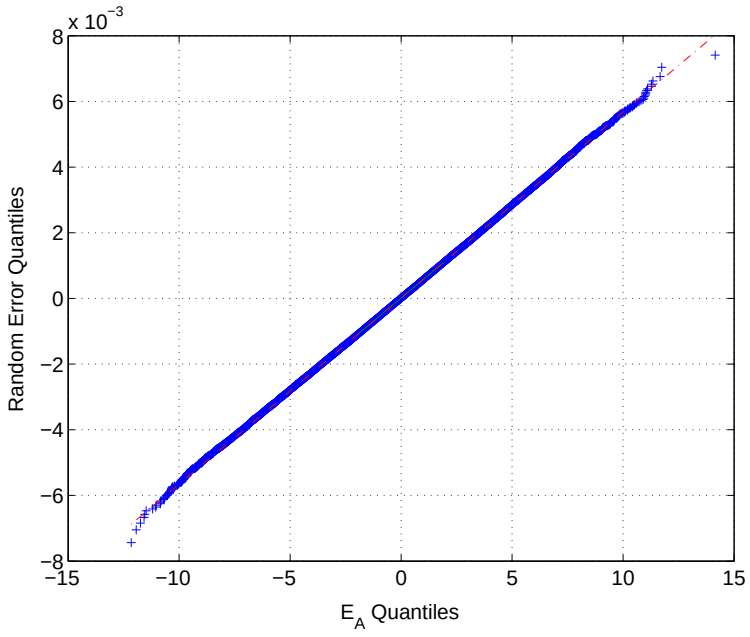

Figure 3.4: Comparsion of quantiles for E_A, and applied error, in initial position

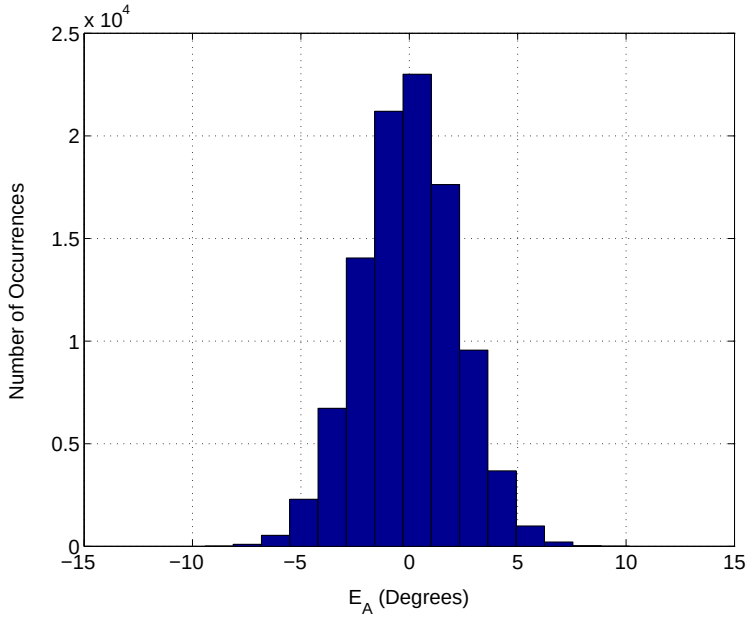

Figure 3.5: Histogram showing E_A for the wing in morphed position

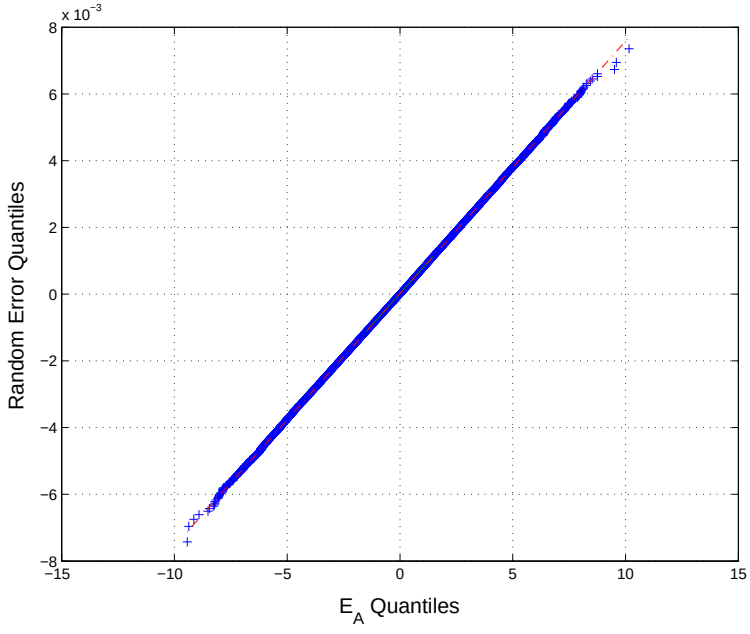

Figure 3.6: Comparsion of quantiles for E_A, and applied error, in morphed position

3.3.2 Linear End Error

The linear error, E_L was also calculated for the input of random manufacturing error. Both E_A and E_L were smaller for the morphed case. Maximum error values are reported in Table 3.1 and histograms of these errors are shown in Figures 3.7 and 3.9. The $Q-Q$ plots for the linear error, and input machining error, again show the relationship of normal distributions.

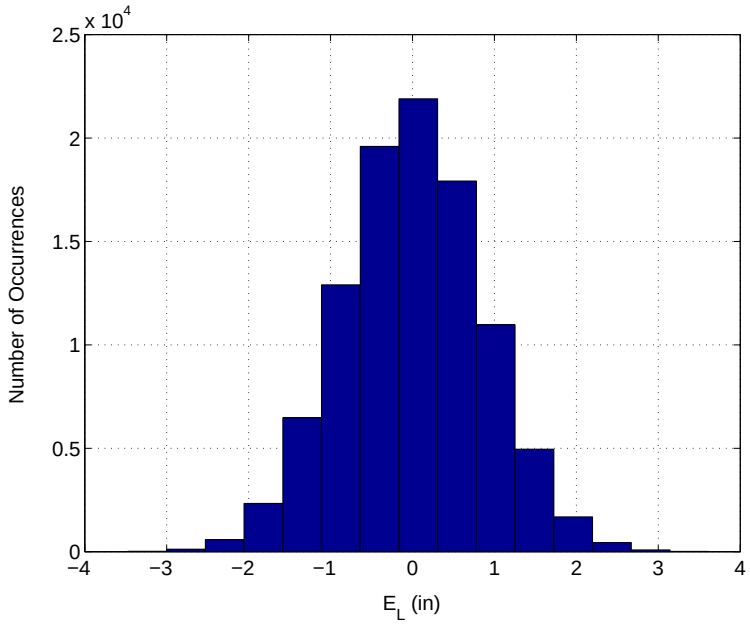

Figure 3.7: Histogram showing E_L for the wing in initial position

3.4 Conclusions of Sensitivity Analysis

Is the QBCLM wing design sensitive to errors in manufacturing? Yes, the wing design is sensitive to errors in manufacturing. However, it is proposed that these errors are acceptable, are inherent in most designs for morphing aircraft, and can be minimized with proper actuation and control schemes.

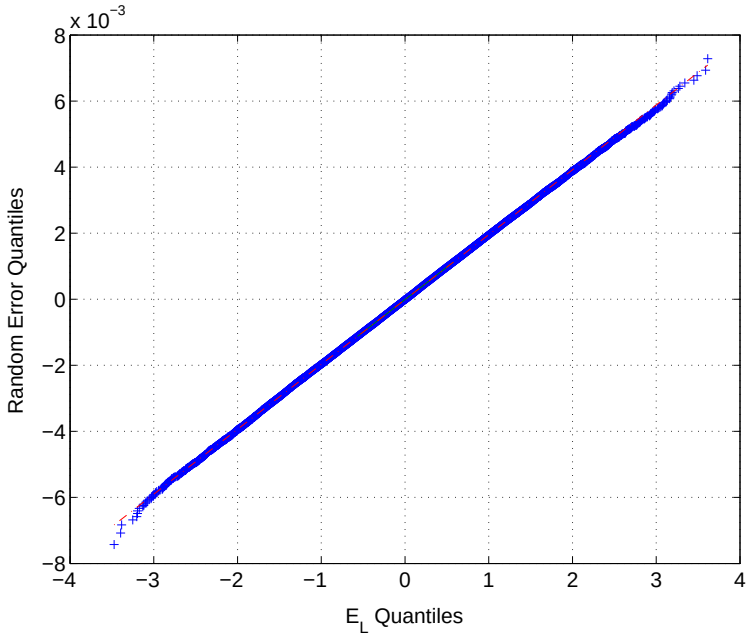

Figure 3.8: Comparison of quantiles for E_L, and applied error, in initial position

The simulated manufacturing error was chosen as a conservative value. Current manufacturing processes can generate parts with higher accuracy and repeatability than the simulations allowed. Yet, even with the large values of simulated manufacturing error, the output error was both predictable (having the same distribution) and remarkably low (between zero and three inches of error at a span of over seven feet).

It is also assumed that proper actuation and feedback control techniques would be developed. These tools, working together, could enable error to measured while the vehicle is in flight, and to adjust the placement of the wing as temperature and wind loading vary.

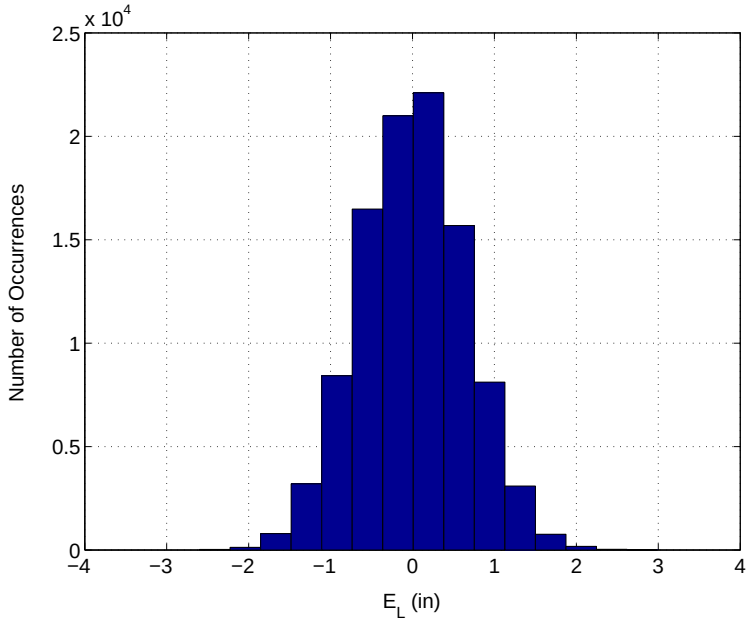

Figure 3.9: Histogram showing E_L for the wing in morphed position

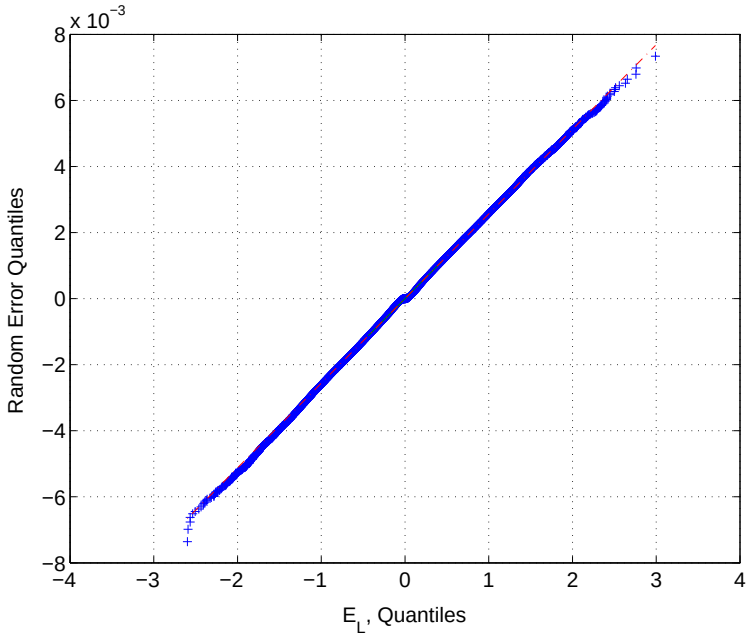

Figure 3.10: Comparison of quantiles for E_L, and applied error, in morphed position

Chapter 4

Conclusions and Future Work

4.1 Conclusions

In order to improve energy efficiency, flight control and mission control, concepts for morphing aircraft must be developed. Quite a number of concepts have been generated, many of which are too complex to be implemented in the near future. Most of these concepts employ multiple degrees of freedom and have proven to be too bulky or too difficult to control.

One of NASA's biologically inspired wing designs has proved very efficient in wind tunnel tests, beating a planar elliptical wing by 15 percent in lift-to-drag comparisons of wings with similar wingspans and aspect ratios. This hyper-elliptic cambered span (HECS) wing design appears to be very promising in flight. However, a method of morphing this wing between a planar hyper-elliptical shape, and a morphed non-planar hyper-elliptical shape is desired.

A novel single degree of freedom mechanism has been developed for morphing along the entire span of an aircraft wing. This concept has been shown to be feasible from both kinematic and mechanical design viewpoints. In fact, it is possible to employ one actuator to control both wings, morphing both of them between the initial and final desired shapes.

The kinematic synthesis tools developed for the hyper-elliptic cambered span wing can be applied to any wing shape or configuration. It has been shown how dimensions of the mechanism can be synthesized (see section 2.4), how chord sections can be placed (see Appendix A), and how wing sweep can be accommodated (see section 2.6).

Using the synthesis tools developed, the mechanism can match the required shape exactly at any number of specified points along the span. Matching of more complex curves, or additional specified intermediate positions, might also be accomplished through multiple degrees of freedom gained by rigid link actuation.

Due to the large shape change generated by relatively small actuation, the sensitivity of this mechanism to random errors in link manufacturing was also addressed. The response error due to practical machining errors was enumerated, and shown to be small.

4.1.1 Author's contributions

The project described was a team effort. The contributions provided by the author include the following:

1. Involvement in conceptual design
    - Involved in design discussions
    - Co-developed initial synthesis
2. Development of swept design
    - Developed swept synthesis
    - Developed swept design
    - Responsible for swept model construction
3. Development of sensitivity analysis
4. Development of "Chord Section Placement" optimization code

4.2 Future Work

Now that the mechanism design problem has been solved, some type of skin is needed to form an air/structure interface. The mechanism provides excellent attachment points for the airfoil sections, placing them in the optimum position to resist aerodynamic loading along the span of the wing. However, no skin material has been found that would be suitable for the motion of the wing.

Alternatively, rigid sections may be constructed with covered joints between the sections. Similar joints have already been constructed for use with wing sweep (the F-14 Tomcat is an example, using joints for wing sweep).

Further work is also necessary to address the combination of structural integrity and motion generation. Ideally, some type of topology optimization would be created incorporating both the kinematic and force constraints. This would allow the structure to be optimized in carrying flight loads. The constraints placed on the mechanism design in sections 2.4 were helpful, but could be improved for further structural optimization.

Bibliography

[1] Bowman, J., et al. "Evaluating the impact of morphing technologies on aircraft performance" *43rd AIAA/ASME/ASCE/AHS/ASC Structures, Structural Dynamics, and Materials Conference*. Denver, Colorado, April 22-25, 2002.

[2] Buhl, T. "Design of non-linear mechanisms - topology and shape optimization", Technical University of Denmark. Ph.D. Dissertation. November, 2002.

[3] Davidson, J., et al. "Flight dynamic simulation assessment of a morphable hyper-elliptic cambered span winged configuration" *AIAA Atmospheric Flight Mechanics Conference and Exhibit*. Austin, Texas, August 11-14, 2003.

[4] Erdman, A.G., and G.N. Sandor. *Mechanism Design: Analysis and Synthesis*. 3rd ed. Upper Saddle River: Prentice-Hall, 1997.

[5] Jardine, P., et al. "Smart wing shape memory alloy actuator design and performance" *Proceedings of SPIE - Industrial and commercial applications of smart structures technologies*. Vol. 3044.

[6] Krovi, V., et al. "Kinematic and kinetostatic synthesis of planar coupled serial chain mechanisms," *ASME Journal of Mechanical Design*, Vol. 124, June 2002, pp. 301-312.

[7] Mabie, H.H., and Reinholtz, C.F. *Mechanisms and dynamics of machinery*. 2 Ed. New York: John Wiley & Sons, 1987.

[8] Monner, H.P., "Realization of an optimized wing camber by using formvariable flap structures" *Aerospace Science and Technology*, Vol. 5, Oct. 2001, pp. 445-455.

[9] Quackenbush, A., et al. "Implementation of vortex wake control using SMA-actuated devices" *Proceedings of SPIE - Industrial and commercial applications of smart structures technologies*. Vol. 3044.

[10] Salerno, R. "Position control strategies for a modular, long-reach, truss-type manipulator", Virginia Polytechnic Institute and State University. Ph.D. Dissertation. November 1993.

[11] Salerno, R. "Shape control of high degree of freedom variable geometry truss manipulator", Virginia Polytechnic Institute and State University. M.S. Thesis. 1989.

[12] Saggere, L. "Static shape control of smart structures using compliant mechanisms" *AIAA Journal*, Vol. 37, No. 5, May 1999, pp. 572-78.

[13] Sigmund, O. "On the design of compliant mechanisms using topology optimization," *Mechanics of Structures and Machines*, Volume 25, No. 4, 1997, pp. 493-524.

[14] Stewart, D. "A platform with six degrees of freedom," *Proceedings of the Institute of Mechanical Engineers*, Vol. 180, Part 1, No. 15, 1965-1996, pp. 371-386

[15] Tsai, L-W. "Design of tendon-driven manipulators," *ASME Journal of Mechanical Design*, Vol. 117, June 1995, pp. 80-86.

[16] Tsai, L-W. *Mechanism Design: Enumeration of Kinematic Structures According to Function*. Boca Raton: CRC Press, 2001.

[17] Ulsamer, E. "On the threshold of 'nonclassical' combat flying" *Air Force Magazine*. pp. 54-58, June, 1997.

[18] Whittier, W. "Kinematic Analysis of Tensegrity Structures", Virginia Polytechnic and State University. M.S. Thesis. November, 2002.

[19] Wiggins, L., et al. "Design and analysis of a morphing hyper-elliptic cambered span (HECS) wing" *45rd AIAA/ASME/ASCE/AHS/ASC Structures, Structural Dynamics, and Materials Conference* (to be submitted as AIAA-2004-1885) 2004.

Appendix A

Chord Section Placement

The problem of placing section articulating points along the half-span is developed in the following manner: Assume that a desired shape is given, in this case the hyper-elliptic shape of the anhedral (the initial shape does not require any special placement of sections). Also given are a finite number of sections into which the half-span is to be divided. The placement of the chord sections is an important characteristic of the overall design of the morphing wing. The placement determines the "quality" of the approximation of the mechanism, and it can have significant aerodynamic effects. The "quality" can be defined in a number of ways.

A.1 Quality of Approximation

Defining hyper-elliptic shape as $H(y)$, and piece-wise continuous curve as $L(y)$ (see Figure A.1), the "quality" can be maximized by doing one of the following:

- Minimize the error area (area between $H(y)$ and $L(y)$)
- Maximize area under $L(y)$ (turn problem above into a maximization problem)

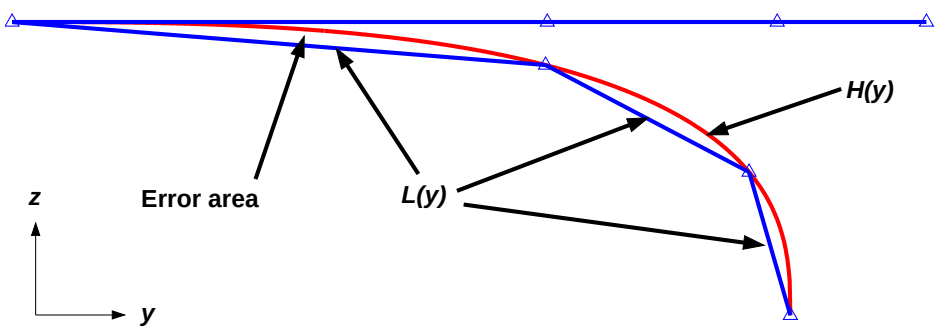

Figure A.1: Definition of $L(y)$ and $H(y)$

- Minimize largest deviation between $L(y)$ and $H(y)$
- Minimize the mean-square error defined as

$$\int [f(x) - l(x)]^2 dx \tag{A.1}$$

- Minimize based on a curvature model (Relate curvature to "section density" to apply sections more frequently when curvature increases)
- Optimize based on some dependent function or aerodynamic formulae (choose a formula that depends on $L(y)$ and optimize based on this)

In this case, the author chose to optimize the placement of chord sections by determining the largest deviation between $L(y)$ and $H(y)$, and causing each section to have equivalent small deviations. This was accomplished by choosing an arbitrary number of sections, allowing each section articulation point to slide freely along the half span (assuming the end points were fixed) until the maximum deviations of the sections were equal. The problem layout is shown in Figure A.2, with section articulating points labeled P_k, and maximum deviations denoted as δ_k. Note that these maximum deviations were taken perpendicular to $H(y)$, at all points to retain physical meaning.

A.2 Algorithm

An algorithm was developed to optimize the placement of chord sections according to the aforementioned method. The example in Figure A.2 will be used to demonstrate the method of section placement chosen.

It was necessary to develop a cost function to describe the deviation, δ, of each section. In this respect, three functions were considered:

$$\Phi_1 = \delta_1 + \delta_2 + \delta_3 \tag{A.2}$$

$$\Phi_2 = \delta_1 + \delta_2 + \delta_3 + |\delta_1 - \delta_2| + |\delta_2 - \delta_3| \tag{A.3}$$

$$\Phi_3 = \delta_1 + \delta_2 + \delta_3 + Max\ Diff \tag{A.4}$$

where

$$Max\ Diff = \max \delta_i \qquad \text{for } i = 1, 2, \ldots, n \tag{A.5}$$

and n is the total number of sections (in this case, $n = 3$).

When minimized, the three functions accomplish different tasks. Φ_1 tends minimize the total deviation, without respect to the equivalence of deviations δ_1, δ_2, and δ_3. Φ_2, on the other hand, by taking into account the relative differences in deviation, tends to keep all δ's approximately equal. Finally, when minimized, Φ_3, tends to keep all δ's approximately

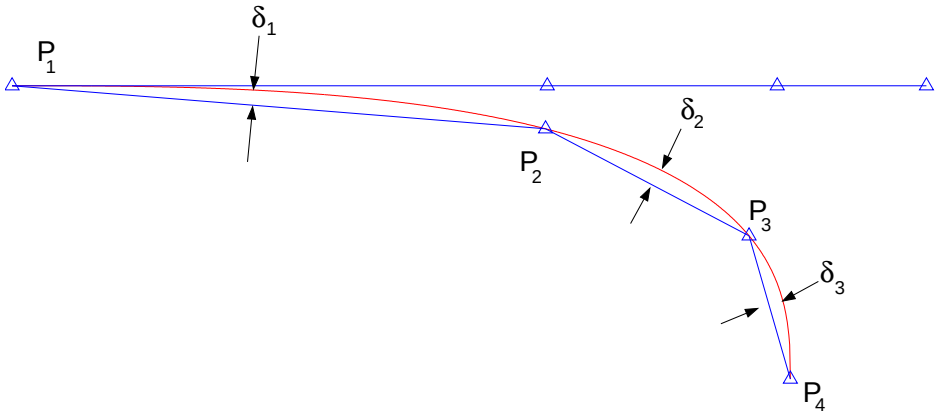

Figure A.2: Definition of Chord Placement

equal, while at the same time spreading the section articulating points evenly over the function.

Φ_3 was chosen as the cost function, and was minimized the following way. A numerical derivative was taken of the cost function with respect to each free articulating point, in this case, P_2, and P_3. This derivative is expressed as

$$\frac{\partial \Phi}{\partial P_2} = f(\delta_1, \delta_2, |\delta_1 - \delta_2|, |\delta_2 - \delta_3|) \tag{A.6}$$

$$\frac{\partial \Phi}{\partial P_3} = f(\delta_2, \delta_3, |\delta_1 - \delta_2|, |\delta_2 - \delta_3|) \tag{A.7}$$

A version of Hook and Jeeves optimization was applied to these derivatives to find the best placement. Some examples are shown in Figures A.3 through A.7.

A.3 Chord Section Optimization Code

The Hook and Jeeves code[1], is included here for reference.

MWHook.m

```
%MWHook.m
%=====================================================================
% This is the main Chord Section Placement Program
% Matthew Stubbs (Summer 2003)
%
%
% Chord Sections are placed based on Hook optimization.
%
% INPUT:
%
% FUNCTIONS: Calls MWCost (Cost Function Definition)
%                  MWHECSPlot (Plot Function)
%
% OUTPUT:
```

[1] Adapted from an in-class handout from Dr. C.F. Reinholtz

```
%=========================================================================
%-------------------------------------------------------------------------
% Initialize
%-------------------------------------------------------------------------
clear all
close all
clc
%-------------------------------------------------------------------------
% Define Number of Sections
%-------------------------------------------------------------------------
Sections=3;
%-------------------------------------------------------------------------
% Define Initial Points and Parameters
%-------------------------------------------------------------------------
Py(1)=0;
Py(Sections+1)=13;

param = zeros(1,Sections+1);
newparam = zeros(1,Sections+1);

%-------------------------------------------------------------------------
% OPTIMIZATION
%-------------------------------------------------------------------------
%   Initial Drop into design space
%-------------------------------------------------------------------------
for jj=2:Sections
    Py(jj)=(jj-1)/Sections*Py(Sections+1);
end
param(1) = Py(1);
for jj=2:Sections
    param(jj)=Py(jj);
end
param(Sections+1)=Py(Sections+1);
%-------------------------------------------------------------------------
%   Set step size (these are the starting delta section placement)
%-------------------------------------------------------------------------
StepSize = [0 ones(1,Sections-1) 0];
OStepSize = StepSize;
%-------------------------------------------------------------------------
%   Compute current cost function and check parameters
%-------------------------------------------------------------------------
CurrentCost = MWCost(param,Sections);
```

```
%-------------------------------------------------------------------------
%   Not good programming practice
%   However yields starting values for initial comparison
%-------------------------------------------------------------------------
OldCost = 1000000;
CostDifference = 0.00001;
StepCheck = 0.01*ones(1,Sections+1);
iteration=0
%-------------------------------------------------------------------------
% START OPTIMIZATION LOOP
%-------------------------------------------------------------------------
while abs(OldCost-CurrentCost) > CostDifference | sum(StepCheck<StepSize)>0

newparam=param;

OldCost = CurrentCost;
%-------------------------------------------------------------------------
%   EXPLORATORY SEARCH, the steps have a magnitude (stepsize) and a + or
%   - sense determined by the Direction vector.  During the exploratory
%   loop below, the direction may also be set to zero to indicate that
%   neither a plus or a minus step in that direction lowered the cost.
%-------------------------------------------------------------------------

Direction = [0 ones(1,Sections-1) 0];
%-------------------------------------------------------------------------
%      step in each direction and check for improvements
%          (set Direction(j)= 0 is both directions fail)
%-------------------------------------------------------------------------
for j=1:Sections+1
 newparam(j) = param(j)+StepSize(j)*Direction(j);
 NewCost = MWCost(newparam,Sections);
   if NewCost > CurrentCost
    Direction(j) = -Direction(j);
    newparam(j) = param(j)+StepSize(j)*Direction(j);
    NewCost = MWCost(newparam,Sections);
    if NewCost > CurrentCost
      Direction(j) = 0;
      StepSize(j) = StepSize(j)/2;
     end
  end
end
%   End of the Exploratory Search
```

```
move = StepSize;

%-------------------------------------------------------------------
% Start the PATTERN MOVE
%-------------------------------------------------------------------
newparam = param + StepSize.*Direction;
newcost = MWCost(newparam,Sections);

while newcost < CurrentCost
   param = param + move.*Direction;
   CurrentCost = newcost;
   move = move*1.25;
   newparam = param + move.*Direction;
   newcost = MWCost(newparam,Sections);

end
iteration=iteration+1
end
param
newcost
MWHECSPlot(param,Sections)
```

MWCost.m

```
%MWCost.m
%===================================================================
% This is the cost function called by Hook and Jeeves optimization
% Matthew Stubbs (07.30.03)
%
%
%
% INPUT:   Parameters, and number of Sections
%
%
% OUTPUT:  Cost of parameters based on 'Max Delta' technique
%===================================================================
%-------------------------------------------------------------------
% Initialize
%-------------------------------------------------------------------

function [Cost]=MWCost(param,Sections)
```

```
Py=param;
Pz=MWHECS(Py);
P=Py+i*Pz;
%-------------------------------------------------------------------------
% Insert parameters into MWHECS function
%   MWHECS is considered proprietary, and yields information
%   about the hyper-elliptic curve
%-------------------------------------------------------------------------
for jj=1:Sections
    m=(imag(P(jj+1))-imag(P(jj)))/(real(P(jj+1))-real(P(jj)));
    y=linspace(real(P(jj)),real(P(jj+1)),1000);
    Z=MWHECS(y);
    L=MWHECSLine(y,m,P(jj));
    delta_z(jj,:)=Z-L;
    delta(jj,:)=delta_z(jj,:)/sqrt(m^2+1);
    max_delta(jj)=max(delta(jj,:));
end
%-------------------------------------------------------------------------
% COST FUNCTION
%-------------------------------------------------------------------------
FirstCost=sum(max_delta);
if FirstCost==NaN
    Cost=100;
else
    Cost=FirstCost;
end
max_delta;
```

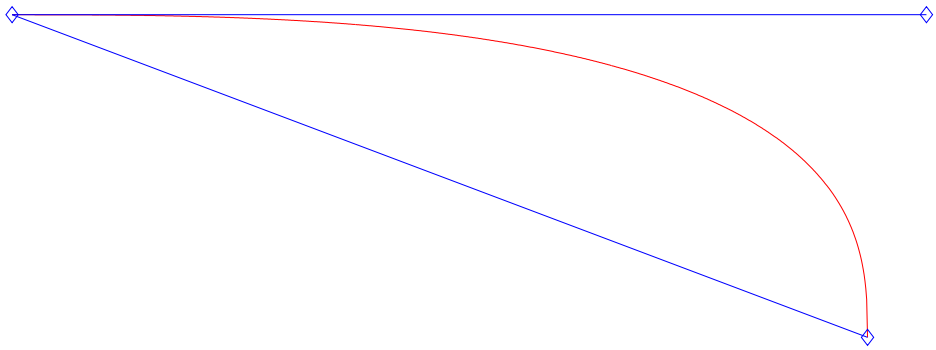

Figure A.3: Example of optimization output: $n = 1$

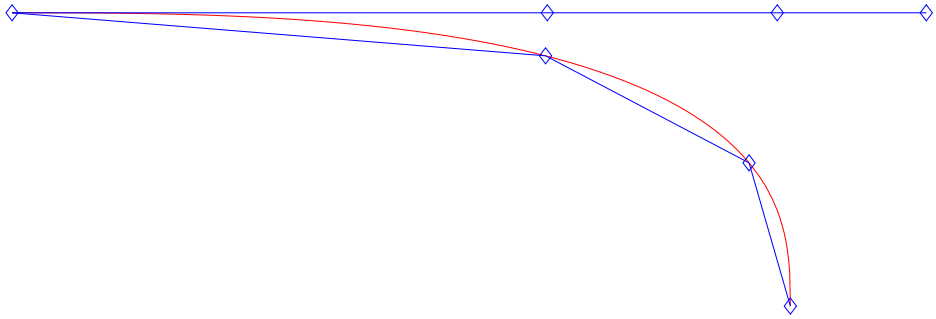

Figure A.4: Example of optimization output: $n = 3$

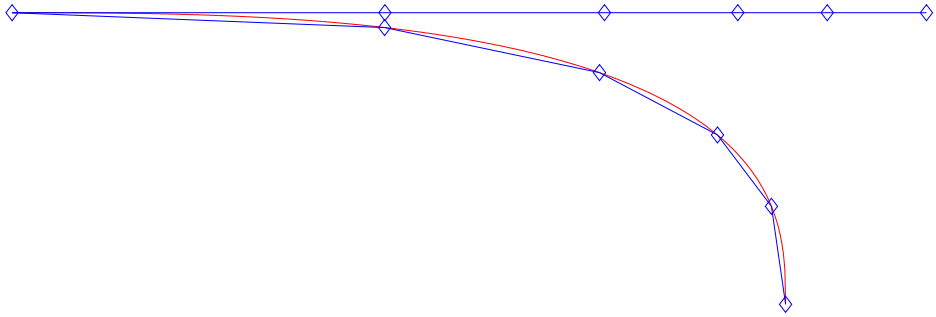

Figure A.5: Example of optimization output: $n = 5$

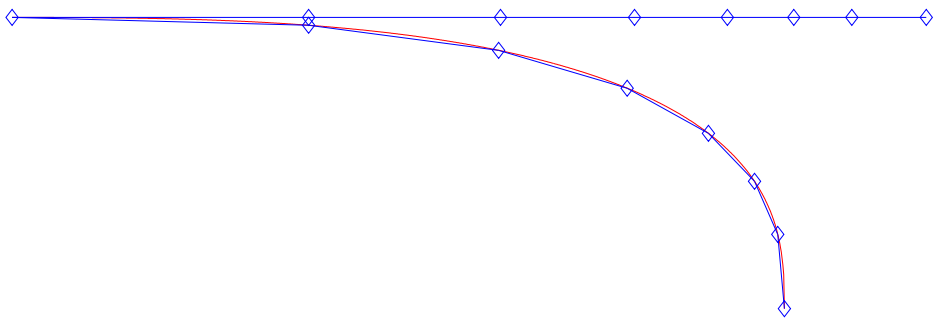

Figure A.6: Example of optimization output: $n = 7$

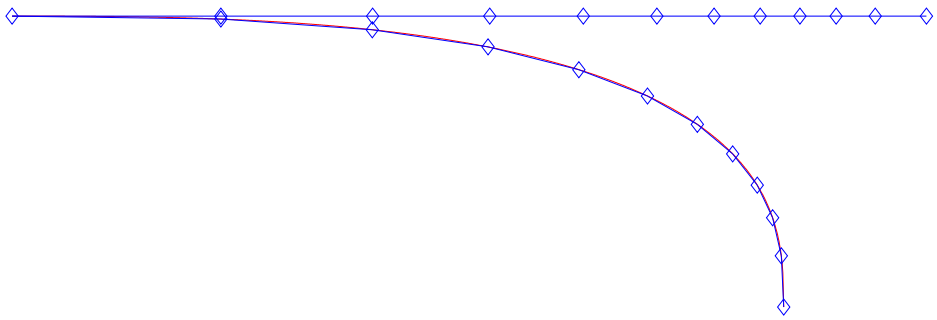

Figure A.7: Example of optimization output: $n = 11$

Appendix B

Mechanism Synthesis Code

B.1 MWPivot.m

```
%=====================================================================
% This is the main Morphing Wing Pivot Arm design program
% Will Whittier (Fall 2002)
%
% Code adapted, and comments:
% Matthew Stubbs (Summer 2003)
%
% Synthesis of HECS wing QBCLM parameters.  Dimensions are read from
% input file.  These dimensions are proprietary information and are
% not included.
%
% INPUT:   MWPivotDimen (Necessary dimensions from NASA Langley)
%
% FUNCTIONS: Calls MWPivotCables (root finding)
%
% OUTPUT:
%=====================================================================
%---------------------------------------------------------------------
% Initialize
```

```
%-----------------------------------------------------------------------
clear all
close all
clc
%-----------------------------------------------------------------------
% Get Dimensions from the Dimension file
%-----------------------------------------------------------------------
[Theta,ThetaT,CDistance,FDistance,ChordH,ChordL,LdEdge]=MWPivotDimen;
%-----------------------------------------------------------------------
% Find Cross link Attachment Information for sections
%-----------------------------------------------------------------------
for n=2:11
    %-------------------------------------------------------------------
    % Assign variables to the dimensions from MWPivotDimen
    %-------------------------------------------------------------------
    S=CDistance(n-1);
    Sb=CDistance(n);
    c0=ChordH(n-1);
    cA=ChordH(n);
    cB=ChordH(n+1);
    ThetaA=Theta(n-1);
    ThetaB=Theta(n);
    fig=n;
    znlegend=1;
    %-------------------------------------------------------------------
    % Call MWPivotCables (root finding)
    %-------------------------------------------------------------------
    [P,yAP,zAP,yRB,zRB]=...
        MWPivotCables(S,Sb,c0,cA,cB,ThetaA,ThetaB,fig,znlegend);
    Pr(n-1,1:3)=P;
    yAPr(n-1)=yAP;
    zAPr(n-1)=zAP;
    yRBr(n-1)=yRB;
    zRBr(n-1)=zRB;
end
%-----------------------------------------------------------------------
% Save the workspace variables needed to move the Wing from the
% starting position through intermediate points to the final position
%
% These variables are called later for numerous programs including
% Sensitivity Analysis (Stubbs)
%-----------------------------------------------------------------------
```

```
save MoveV Theta CDistance FDistance ChordH ChordL LdEdge...
        yAPr zAPr yRBr zRBr
```

B.2 MWPivotCables.m

```
%MWPivotCables.m Function
%-------------------------------------------------------------------
% This is the root finding function called by MWPivot
% Will Whittier (Fall 2002)
%
% Code adapted, and comments:
% Matthew Stubbs (Summer 2003)
%
%
% INPUT:   S,sB,c0,cA,cB,ThetaA,ThetaB,fig,znlegend
%
% FUNCTIONS: Calls fzero, MWPivotDraw
%
% OUTPUT:  P,yAp,zAp,yRB,zRB to MWPivot
%-------------------------------------------------------------------
%-------------------------------------------------------------------
%   Initialize
%-------------------------------------------------------------------
function [P,yAp,zAp,yRB,zRB]=...
        MWPivotCables(S,sB,c0,cA,cB,ThetaA,ThetaB,fig,znlegend)
%-------------------------------------------------------------------
% ROOT FINDING
%-------------------------------------------------------------------
%-------------------------------------------------------------------
%   Set Initial Guess
%-------------------------------------------------------------------
zA0=cA/2;
%-------------------------------------------------------------------
%   Set Variables
%-------------------------------------------------------------------
yRB=0;
zRB=-cB/2;
if cB==0
    zRB=-(cA)/2;
end
%-------------------------------------------------------------------
```

```
%   Create Function Handle
%-------------------------------------------------------------------------
F=@MWPCFun;
%-------------------------------------------------------------------------
%   Set Options
%-------------------------------------------------------------------------
options=optimset('TolX', 1e-12);
%-------------------------------------------------------------------------
%   Initialize Counter
%-------------------------------------------------------------------------
n=0;
%-------------------------------------------------------------------------
%   Try different y locations of attachment point (I)
%-------------------------------------------------------------------------
for yA=0:S/1e2:S,
    %---------------------------------------------------------------------
    %   Increment Counter
    %---------------------------------------------------------------------
    n=n+1;
    %---------------------------------------------------------------------
    %   Solve for z location of cable attachment point to get the
    %   desired change in length using the numerical root finder
    %---------------------------------------------------------------------
    [zA]=fzero(F,zA0,options,yA,zRB,yRB,S,cA,cB,ThetaA,ThetaB);
    %---------------------------------------------------------------------
    %   Record Points
    %---------------------------------------------------------------------
    yAr(n)=yA;
    zAr(n)=zA;
end
yAp=yAr(1);
zAp=zAr(1);
```

Appendix C

Position Analysis

C.1 Derivation

The position of any point of the QBCLM can be found using a variety of approaches. One approach is to apply the law of cosines and the law of sines to find the unknown angles of links 3 and 4 (it is assumed that the positions of links 1 and 2 are specified). This method is used to find the angular position of all links within a section of the mechanism. To find the position of the links of any section k, $k \neq 1$, the positions of the previous sections, $n = 1, 2, \ldots, k$, must be found first.

If the link lengths, L_i, input angle (θ_2) and ground position (θ_1) of a mechanism are known, the remaining angles of θ_3 and θ_4 can be found. Consider the QBCLM given in Figure C.1. For this mechanism, loop closure is performed by writing a vector loop equation for the four links. This vector equation is then solved for the only two unknowns θ_3 and θ_4.

The loop closure equation for this mechanism is

$$r_2 e^{j\theta_2} + r_3 e^{j\theta_3} + r_4 e^{j\theta_4} + r_1 e^{j\theta_1} = 0 \tag{C.1}$$

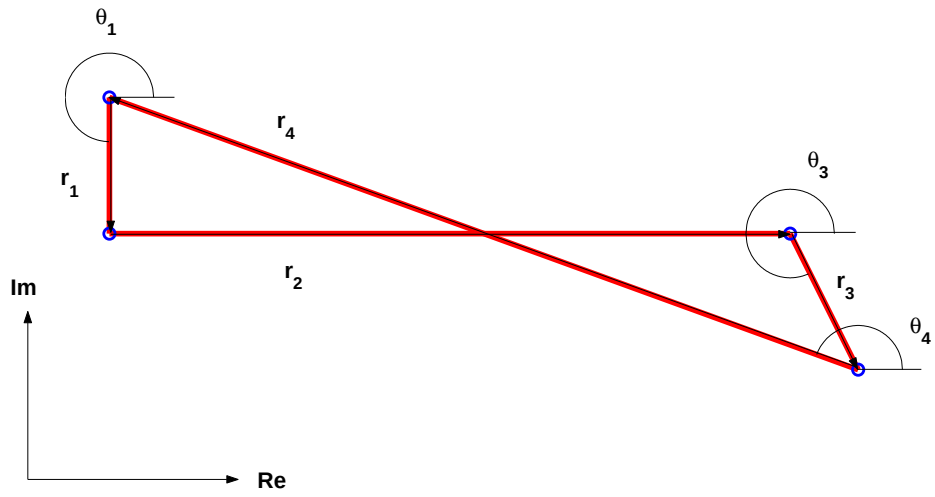

Figure C.1: An example section extracted from the QBCLM

The vectors $\overrightarrow{r_1}$ and $\overrightarrow{r_2}$ are fully known. Separating the loop closure equation into known and unknown parts yields a known vector that simplifies the solution by reducing the geometry to triangles:

$$r_g e^{j\theta_g} = r_2 e^{j\theta_2} + r_1 e^{j\theta_1} = -r_4 e^{j\theta_4} - r_3 e^{j\theta_3} \tag{C.2}$$

The vector, $\overrightarrow{r_g}$, is known from the given angles and link lengths. The known vector and the resulting triangle are shown in Figure C.2.

Applying the law of cosines to the triangle $\overrightarrow{r_3}$, $\overrightarrow{r_4}$, $\overrightarrow{r_g}$, yields Equation C.3 that will be used to solve for β.

$$r_g^2 = r_4^2 + r_3^2 - 2r_4 r_3 \cos\beta \tag{C.3}$$

where β is the acute angle between $\overrightarrow{r_3}$ and $\overrightarrow{r_4}$. Solving for β yields

$$\beta = \cos^{-1}\left[\frac{r_g^2 - r_4^2 - r_3^2}{-2r_4 r_3}\right] \tag{C.4}$$

Applying the law of cosines to the triangle $\overrightarrow{r_3}$, $\overrightarrow{r_4}$, $\overrightarrow{r_g}$, yields Equation C.5 that will be used to solve for α.

$$r_4^2 = r_g^2 + r_3^2 - 2r_g r_3 \cos\alpha \tag{C.5}$$

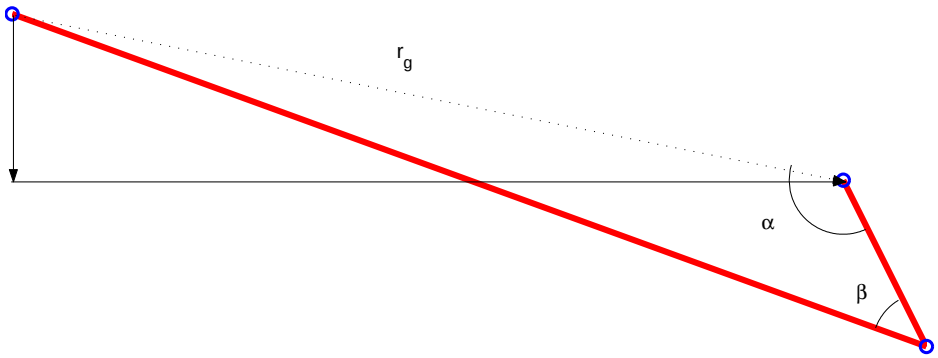

Figure C.2: Definition of α and β

where α is the acute angle between $\overrightarrow{r_3}$ and $\overrightarrow{r_4}$. Solving for α yields

$$\alpha = \cos^{-1}\left[\frac{r_4^2 - r_g^2 - r_3^2}{-2r_g r_3}\right] \tag{C.6}$$

Now, note that the relationship between θ_3, θ_4, α, and β changes when the mechanism is in a different closure. For our use, we are solving for what is usually thought of as the second closure. For this closure, the relationships (from Figure 4) are that

$$\theta_3 = 180\,^\circ + \theta_g + \alpha \tag{C.7}$$

$$\theta_4 = 180\,^\circ + \theta_3 + \beta \tag{C.8}$$

C.2 Position Analysis of Unswept QBCLM

Once, θ_3 and θ_4 of a section are known, one can obtain the $y - z$ position of any point on the mechanism in a straight forward manner. For example, to find the position of the node where the chord section will be placed (at the joint between links 2 and 3 – see Figures A.2

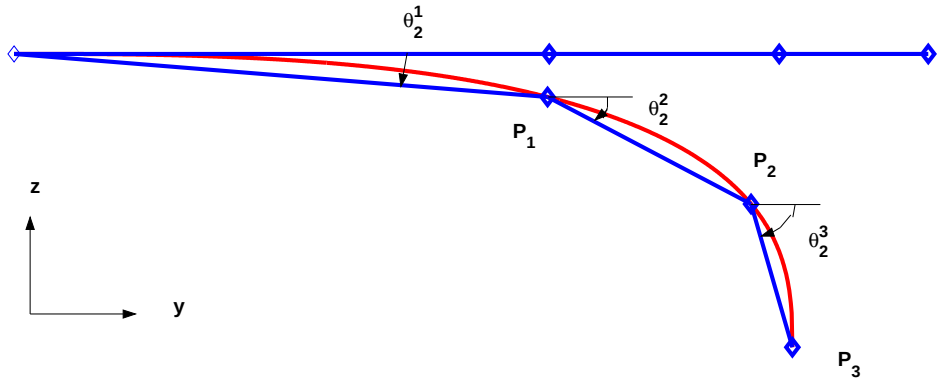

Figure C.3: Example for position analysis

and C.3), P_2,

$$P(x,y,z) = P_{2x}\hat{i} + P_{2y}\hat{j} + P_{2x}\hat{k} \tag{C.9}$$

$$P(x,y,z) = \begin{cases} P_{2x} = 0 \\ P_{2y} = S_1 \cos\theta_2 \\ P_{2z} = S_1 \sin\theta_2 \end{cases} \tag{C.10}$$

C.3 Including Sweep

$$P(x,y,z) = P_{2x}\hat{i} + P_{2y}\hat{j} + P_{2x}\hat{k} \tag{C.11}$$

$$P(x,y,z) = \begin{cases} P_{2x} = S(y)\sin\phi^k \\ P_{2y} = S_1 \cos\theta_2 \\ P_{2z} = S_1 \sin\theta_2 \end{cases} \tag{C.12}$$

where

$$S(y = S^k) = \sigma^k \tag{C.13}$$

and ϕ^k is the mechanism sweep of section k shown in Figure C.4.

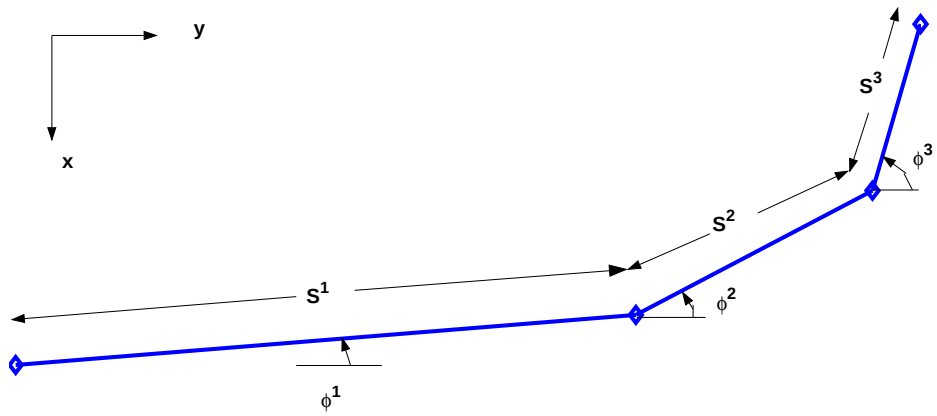

Figure C.4: Planform view of mechanism sweep

Vita

Matthew was born in Birmingham, Alabama on August 9, 1979. He is the son of J. Shelton, and Jan Stubbs, and the brother of Mark Stubbs. Moving often with their family, Matthew and Mark grew up in Monkton, Maryland, and Matthews, North Carolina. During his time in North Carolina, Matthew was home schooled. After their father took a position in Kingsport, TN, both Matthew and Mark attended Tennessee Technological University in Cookeville, and received bachelors' degrees in Mechanical Engineering on the same day. Matthew was married to Ashley Harper of Crossville, TN in December of 2002, after one semester at Virginia Tech. Matthew's Masters degree in Mechanical Engineering was completed in December 2003.